Influence of interfaces on the phonon density of states of nanoscale metallic multilayers: Phonon confinement and localization

W. Keune, Sampyo Hong, M. Y. Hu, J. Zhao, T. S. Toellner, E. E. Alp, W. Sturhahn, T. S. Rahman, and B. Roldan Cuenya

Phys. Rev. B **98**, 024308 — Published 20 July 2018

DOI: 10.1103/PhysRevB.98.024308

Influence of interfaces on the phonon density of states of nanoscale metallic multilayers:

Phonon confinement and localization

W. Keune[1], Sampyo Hong[2,3], M. Y. Hu[4], J. Zhao[4], T. S. Toellner[4], E. E. Alp[4], W. Sturhahn[5], T. S. Rahman[2#], B. Roldan Cuenya[2,6*]

[1]Department of Physics, University of Duisburg-Essen, 47057 Duisburg, Germany

[2]Department of Physics, University of Central Florida, Orlando, FL 32816, USA

[3]Division of Physical Sciences, Brewton-Parker College, Mount Vernon, GA 30445, USA

[4]Advanced Photon Source, Argonne National Laboratory, Lemont, IL 60439, USA

[5]Seismological Laboratory, California Institute of Technology, Pasadena, CA 91125, USA

[6]Department of Interface Science, Fritz-Haber Institute of the Max Planck Society, 14195 Berlin, Germany

E-mail: * roldan@fhi-berlin.mpg.de ; # talat@ucf.edu

Abstract

Isotope-selective ^{57}Fe nuclear resonant inelastic x-ray scattering (NRIXS) measurements and atomic-layer resolved density functional theory (DFT) calculations were used to investigate the effect of interfaces on the vibrational (phonon) density of states (VDOS) of (001)-oriented nanoscale Fe/Ag and Fe/Cr multilayers. The multilayers in the experiment contained isotopically enriched ^{57}Fe monolayers as probe layers located either at the Fe/Ag or Fe/Cr interfaces or in the center of the Fe films. This allows probing of the vibrational dynamics of Fe sites either at the buried interfaces or in the center of the Fe films. For Fe/Ag multilayers, distinct differences were observed experimentally between the Fe-partial VDOS at the interface and in the center. At the Fe/Ag interface, the high-energy longitudinal-acoustic (LA) phonon peak of Fe near ~ 35 meV is suppressed and slightly shifted to lower energy, and the low-energy part of the VDOS below ~ 20 meV is drastically enhanced, as compared to the Fe-specific VDOS in the center Fe layers or in bulk Fe. Similar phenomena are found to a less degree in the Fe/Cr multilayers. The measured Fe-partial VDOS was used to determine Fe site-selective vibrational thermodynamic properties of the multilayers. Our theoretical findings for the layer-dependent VDOS of the multilayers are in qualitative agreement with the experimental results

obtained by NRIXS. For Fe/Ag multilayers, which are characterized by a large atomic mass ratio, the experimental and theoretical results demonstrate phonon confinement in the Fe layers and phonon localization at the Fe/Ag interfaces due to the energy mismatch between Ag and Fe LA phonons. These phenomena are reduced or suppressed in the Fe/Cr multilayers with their about equal atomic masses. Moreover, direction-projected Fe-VDOS along the (nearly in-plane) incident x-ray beam were computed in order to address the intrinsic vibrational anisotropy of the Fe/Ag multilayer. We have also performed spin-resolved electronic band structure (DFT) calculations, predicting an enhanced magnetic moment ($\mu_{Fe} = 2.8\ \mu_B$) of the interfacial Fe atoms and a high electron spin polarization (79 %) at the Fermi energy for the Fe/Ag interface, as compared to the case of Fe center layers. This is a result of charge transfer from Fe to Ag at the interface. On the contrary, Cr tends to donate electrons to Fe, thus reducing the interfacial Fe moment ($\mu_{Fe} = 1.9\ \mu_B$). This implies strong chemical bonding at the Fe/Ag and Fe/Cr interfaces, affecting the interfacial VDOS.

I. Introduction

In quest of the nature of the vibrational (phonon) spectrum in two-dimensional (2D) solids, such as nanoscale multilayers (or superlattices) and their interfaces, intriguing phenomena have been observed in the last decades [1], which have no counterpart in the corresponding bulk materials. A multilayer is an artificial periodic structure made by alternately stacking of nanoscale thin films, A and B, of different elastic materials with different Debye temperatures and with different atomic masses. The discovered phenomena imply Brillouin zone folding of acoustic phonon modes, phonon confinement, and phonon localization [1]. Zone folding of the dispersion relations E(q) (E = phonon energy, q = phonon quasi-momentum) may appear because of the artificial periodicity of the multilayer structure [1], and may result in phonon energy band gaps in the Brillouin zone for such nanoscale 'hypersonic phononic crystals' [2,3]. In phonon confinement, no propagating phonon mode is allowed in one of the constituent thin-film layers, A or B, whereas phonon localization implies vibrational modes with a limited number of vibrating atoms, e.g., at the interface between the constituents [1]. As compared to the properties of the bulk materials A and B, zone folding, confinement and localization in multilayers leads to modification of the phonon dispersion relations and of the phonon spectrum, i.e. of the vibrational (phonon) density of states (VDOS), g(E) [4]. These modifications have impact on the vibrational thermodynamic properties, such as, e.g., the vibrational specific heat C and vibrational entropy S, which are connected to g(E) by well-known thermodynamic relations [5-8]. In addition, phononic transport, i.e., the phonon thermal conductivity κ, in nanoscale periodic structures, including multilayers, has become of particular interest [4,9-11], because materials with low thermal conductivity are employed in modern technologies, e.g., in superlattice thermoelectric devices [12-14]. Balandin and Wang [15] predicted the effect of acoustic phonon confinement and corresponding modification of their group velocities on the thermoelectric figure of merit of quantum wells and superlattices. The thermal conductivity is given by the phenomenological kinetic theory expression

[16] $\kappa = (1/3)Cv^2\tau = (1/3)Cv\lambda$ (where C is the vibrational specific heat per unit volume, v is the average phonon velocity or average group velocity, τ is the phonon lifetime and λ is the phonon mean-free path between collisions). Thus, κ is indirectly related to g(E) via the specific heat C and to the group velocity. The interface in multilayers plays an important role, since interface scattering of phonons is a very efficient way of stopping the flow of phonons in multilayers [13,14,17]. In molecular dynamics model calculations by Mizuno et al. [4], who used atomic Lennard-Jones potentials in their computations, the reduction of the thermal conductivity in nanoscale multilayers is attributed to the decrease of the average phonon group velocity (implying a modified VDOS) relative to the bulk and to phonon localization, in addition to interfacial phonon scattering. Thus, the VDOS, modified at the interface between the materials A and B, might be involved in reducing the thermal conductivity in nanoscale multilayers. However, Lennard-Jones potentials [4] are inappropriate to adequately describe the atomic potential in metallic multilayers because of the inherent itinerancy of metal electrons. In a recent study, Dechaumphai et al. [18] demonstrated for nanoscale Au/Si multilayers that the interfacial thermal resistance (ITR) dominates the behavior of cross-plane (perpendicular to the multilayer plane) phonon transport, and that the ITR is dictated by the contrast in acoustic properties of Au and Si, which are phenomenologically characterized by their large Debye-temperature (θ_D) ratio of $\theta_D(Si)/\theta_D(Au) \sim 3.9$. A model, often used for calculating the thermal (phonon) boundary conductance between materials A and B, is the 'diffusive mismatch model' (DMM) [18,19], where the phonon group velocity and the vibrational (phonon) density of states (VDOS) enter as decisive quantities. Reddy et al. [20] pointed out the limitations of the Debye approximation in DMM calculations, and Dechaumphai et al. emphasized the use of DMM-calculated bulk (3-dimensional) full phonon dispersion relations in order to correctly describe the ITR in Au/Si multilayers [18]. However, the use of the bulk phonon dispersion for the interface in A/B multilayers is very problematic, as the phonon DOS in metallic multilayers is known from experiment [21] to depend on the individual nanoscale film thickness as well as on the ratio of the upper phonon cut-off frequencies (i.e., on the phonon contrast) of the two multilayer materials A and B. Therefore, knowledge of the phonon DOS at interfaces becomes of paramount interest for the basic understanding and engineering of low-dimensional devices. The VDOS in nanoscale multilayers, including the VDOS at interfaces, appears to be one of the important quantities for the description of the vibrational thermodynamics and phonon transport in such systems [3, 4]. Furthermore, in order to recognize the significance of solid-solid interfaces, one should notice that interface-induced superconductivity appears to exist in epitaxial FeSe ultrathin films on $SrTiO_3(001)$ substrates [22] and interfacial mode coupling (most probably between optical $SrTiO_3$ phonons and FeSe electrons at the interface) was inferred as the origin of the enhancement of the superconducting transition temperature in FeSe/$SrTiO_3$ [23].

The fundamental question of how the VDOS, g(E), in nanoscale metallic multilayers is modified as compared to bulk materials is rather unexplored and remains an experimental challenge to date. Raman spectroscopy is the method of choice for studying phonons in semiconducting superlattices

[24-27]. A study of nanoscale metallic (Co/Ru) multilayers by Raman spectroscopy was reported by Grimsditch et al. [28], who observed confined optical phonons. However, Raman spectroscopy is sensitive to long wavelength phonons only, and cannot be used to determine g(E). This applies also for Brillouin light scattering, which revealed localized phonon modes due to interface-induced modifications of elastic force constants in metallic multilayer structures [29-31]. The classical method of inelastic neutron scattering remains a challenge because of insufficient sensitivity. First-principles calculations [32] for monolayer-scale Fe(001)/Au(001) superlattices predicted drastic variations of g(E) with t_{Au} and t_{Fe}, where t is the individual layer thickness.

In the present work we employ isotope-selective ^{57}Fe nuclear resonant inelastic x-ray scattering (NRIXS) measurements, supported by atomic-layer resolved first-principles density-functional-theory (DFT) based calculations, in order to investigate the impact of interfaces on the vibrational (phonon) density of states of (001)-oriented Fe/Ag or Fe/Cr nanoscale metallic multilayers. The multilayers in the experiment carried isotopically enriched ^{57}Fe monolayers as probe layers located either at the Fe/Ag or Fe/Cr interfaces or in the center of the otherwise ^{56}Fe films. This allows probing the vibrational dynamics of ^{57}Fe sites either at the buried interfaces or in the center of the Fe films. We selected the Fe/Ag system because of the different elastic properties of the constituents [atomic mass ratio of $m_{Ag}/m_{Fe} \sim 2$ and bulk Debye temperatures [16] of θ_D(Ag) = 225 K (soft metal) and θ_D(Fe) = 470 K (hard metal), and compared with results on the Fe/Cr system with relatively similar elastic properties of the components ($m_{Cr}/m_{Fe} \sim 1$, θ_D(Cr) = 630 K (hard metal) , θ_D(Fe) = 470 K (hard metal)]. For the Fe/Ag multilayers, distinct differences were observed experimentally between the partial (unprojected) or direction-projected partial Fe-VDOS at the interface and in the center layers. These effects are found to be less pronounced in the Fe/Cr multilayers. Our theoretical findings for the layer-dependent VDOS are found to be in qualitative (for Fe/Ag) and quantitative (for Fe/Cr) agreement with the experimental results obtained by NRIXS. For Fe/Ag multilayers, the experimental and computed results demonstrate phonon confinement in the Fe layers and phonon localization at the Fe/Ag interfaces due to energy mismatch between the Ag and Fe (high-frequency) longitudinal phonons. Further, in the calculations, we investigate the effect of the vibrational anisotropy of the Fe interface layers in the multilayers on the partial Fe-VDOS and compare with experiment. With respect to the influence of interfaces on the VDOS, preliminary results on Fe/Cr(001) superlattices have been reported previously [33].

II. Experimental procedure and sample characterization

A. Sample preparation

A sketch of the sample composition in our experiment and in our DFT calculation is given in Figure 1(a),(b) and Figure 1(c),(d), respectively. Fe/Cr and Fe/Ag multilayers were grown by ultrahigh-vacuum (UHV) deposition of the metals on epi-polished MgO(001) substrates. The

preparation method of our Fe/Cr multilayers is described in detail in Refs.[33-35]. The method for Fe/Ag growth is similar to that for Fe/Cr. The MgO(001) substrates were cleaned using isopropanol before insertion into the UHV chamber. They were heated in UHV at 900 °C for 30 min to remove surface contaminants and to anneal the surface structure. First, a 50-Å thick Cr(001) buffer layer was grown at 670 °C on the annealed MgO(001) surface. Subsequently, the Fe/Ag multilayer was prepared at T_S = 160 °C, which is the same growth temperature as for our Fe/Cr multilayers, and is only slightly lower than the growth temperature of 180 °C used in Ref. [36] to prepare Fe/Ag multilayers by UHV deposition. The pressure during Fe/Ag growth was $1x10^{-9}$ mbar. High purity metals (Ag: 99.999 at.%; ^{57}Fe: 95.5 % isotopically enriched; ^{56}Fe: 99.5 % isotopically enriched; Cr: 99.999 at.%) were evaporated from resistively heated effusion cells with deposition rates of 3.0 Å/min for Ag, 4.2 Å/min for Mössbauer non-active ^{56}Fe, and 1 Å/min for Mössbauer-active ^{57}Fe, as measured by calibrated quartz-crystal oscillators. The multilayers were capped with 50 Å of Cr for protection against oxidation. During molecular beam epitaxy at growth temperatures of 190 – 200°C, nearly no interdiffusion of ^{56}Fe/^{57}Fe was found [37]. Our growth temperature of 160°C is even below this temperature range. Therefore, in our case, ^{56}Fe/^{57}Fe interdiffusion is nearly negligible. We have prepared and studied two types of Fe/Ag samples with individual film thicknesses of t_{Fe} = 13.5 Å (9.4 ML) and t_{Ag} = 16.3 Å (8.0 ML):

MgO(substr.)/Cr(35ML)/[Ag(8ML)/^{57}Fe(0.7ML)/^{56}Fe(8ML)/^{57}Fe(0.7ML)]$_{100}$/Cr(35ML)(cap)

(Fe/Ag "interface" sample)

and

MgO(substr.)/Cr(35ML)/[Ag(8ML)/^{56}Fe(4ML)/^{57}Fe(1.4ML)/^{56}Fe(4ML)]$_{57}$/Cr(35ML)(cap)

(Fe/Ag "center" sample)

(We have used the thickness conversion 1 ML Fe(001) = 1.433 Å, 1 ML Ag(001) = 2.043 Å and 1 ML Cr(001) = 1.442 Å).

As will be shown below, multilayer Fe/Ag "interface" and Fe/Ag "center" samples are characterized by a strong crystallographic Ag(200) texture. In the Fe/Ag interface sample, 0.7 ML thick ^{57}Fe probe layers were deposited at both Fe/Ag interfaces of the 8-ML thick ^{56}Fe layer, and the multilayer period was repeated 100 times. In the Fe/Ag center sample, a 1.4 ML thick ^{57}Fe probe layer was deposited in the center of the 8-ML thick ^{56}Fe layer, and the multilayer period was repeated 57 times. Isotopically enriched ^{56}Fe was used, which gives no nuclear resonance signal. Therefore, the nuclear resonance signal originates only from the isotopically enriched ^{57}Fe probe layers alone, i.e., from the Ag/Fe interfaces in the Fe/Ag interface sample and from the center part of the Fe layers in the Fe/Ag center sample.

We have also investigated epitaxial Fe(001)/Cr(001) multilayers with individual film thicknesses of t_{Fe} = 12.5 Å (8.7 ML) and t_{Cr} = 11.5 Å (8 ML) for comparison with the Fe/Ag multilayers. The Fe(001)/Cr(001) multilayers have the following composition:

MgO(substrate)/Cr(35ML)/[Cr(8ML)/^{57}Fe(0.7ML)/^{56}Fe(8ML)]$_{200}$/Cr(35ML)(cap)

(Fe/Cr "interface" sample)

and

MgO(substrate)/Cr(35ML)/[Cr(8ML)/^{56}Fe(4ML)/^{57}Fe(0.7ML)/^{56}Fe(4ML)]$_{200}$/Cr(35ML)(cap)

(Fe/Cr "center" sample)

In the interface sample, the 0.7-ML thick ^{57}Fe probe layers were only deposited at one of the two types of interfaces, i.e., at the "Fe-deposited-onto-Cr" interface. Some preliminary physical properties of the Fe/Cr multilayers have been reported previously [33-35,38], for instance, their excellent layered structure and their (preliminary) vibrational (phonon) density of states (VDOS).

B. Structural characterization

Crystallographic orientation

The crystallographic structure of the Fe/Ag and Fe/Cr multilayers was investigated by X-ray diffraction (XRD). Figure S1 (see Ref. 39) shows conventional high-angle (Θ - 2Θ) XRD patterns of the two Fe/Ag multilayers (interface and center samples, respectively). These data provide evidence of a pronounced crystallographic (200) texture of the Ag layers in both samples, in agreement with Ref. [36]. There is justification to assume that our thin Fe layers (13.5 Å), deposited at 180 °C, preferably grow with (200)-texture on the (200)-textured Ag films throughout the entire multilayer. This type of orientation is favorable, since the two (200) surface lattices of bcc Fe and fcc Ag are in almost perfect in-plane registry after a mutual rotation of 45° about the surface normal [40], and Fe(200)/Ag(200) epitaxial growth (which often is labeled as Fe(001)/Ag(001) epitaxy) has been often reported in the literature [41-43]. Also, one has to consider in the XRD pattern that the atomic scattering factor (f^2) of Ag is significantly larger than that of Fe [44].

The XRD scans in Fig. S1 (Ref. 39) provide the following lattice parameters (perpendicular to the film plane) for Ag and Fe, respectively: a_{Ag} = 4.061 Å, a_{Fe} = 2.892 Å for the interface sample, and a_{Ag} = 4.071 Å, a_{Fe} = 2.884 Å for the center sample. The lattice parameter of the Ag (Fe) layers in our multilayers is slightly reduced (enhanced) with respect to the value of the bulk material (a_{Ag}(bulk) = 4.086 Å and a_{Fe}(bulk) = 2.866 Å [43]). The ratio a_{Ag}/a_{Fe} is 1.43 for the bulk, and is found to be 1.40 for the interface sample and 1.41 for the center sample. It is known that deviations from the bulk lattice parameters may be found in multilayers [36].

The high-angle XRD patterns of our two Fe(001)/Cr(001) multilayer samples have been presented and discussed previously [33-35] and will not be shown here again. In brief, two symmetrical

superstructure satellite peaks around the Cr/Fe(200) reflection demonstrate the high-quality superlattice structure of our Fe(001)/Cr(001) multilayers. Similar superlattice peaks around the Ag(200) reflection have not been observed for our Fe/Ag multilayers, indicating that the topological layer quality is much better for our Fe/Cr superlattices as compared to the Fe/Ag multilayers.

Multilayer Periodicity

Figure S2 (see Ref. 39) displays the small-angle (Θ - 2Θ) X-ray reflectivity patterns of the multilayers $[Fe(13.5Å)/Ag(16.3Å)]_{100}$ (interface sample) and $[Fe(13.5Å)/Ag(16.3Å)]_{57}$ (center sample), together with a simulation for the ideal [Fe(13.5Å)/Ag(16.3 Å)] multilayer system with homogeneous layers and sharp interfaces. Both samples show only a weak first-order superlattice reflection at $2\Theta \approx 3°$, and no higher-order interferences. The simulated first-order peak approximately coincides with the corresponding measured first-order reflection of both samples. This proves that in the average the nominal Fe-Ag bilayer period (29.8 Å) agrees with the measured bilayer period. However, the absence of measured higher-order reflections demonstrates large interface roughness in our multilayers at such low individual film thicknesses of t_{Fe} = 13.5 Å and t_{Ag} = 16.3 Å . We conclude that the individual Fe and Ag films are no homogeneous films, but possess an island structure, as in similar Fe/Ag multilayers described in the literature [36]. However, we may exclude severe chemical intermixing of Fe and Ag as a reason for the disappearance of higher-order reflections in Fig. S2, as demonstrated by our ^{57}Fe conversion-electron Mössbauer spectra (CEMS) on these samples [see Fig. 2(a),(b)]. The X-ray (θ - 2θ) specular scans shown in Fig. S2 (Ref. 39) provide only a qualitative picture of the Fe/Ag interface roughness. In order to obtain quantitative information on the presumed interfacial island structure sophisticated measurements and modeling of the off-specular diffuse X-ray intensity is required [45], which is beyond the scope of the present work.

As to the Fe(001)/Cr(001) multilayers, representative small-angle reflectivity patters from similar samples show a strong first-order and a weaker third-order low-angle superstructure peak [34]. These observations provide proof of the high superlattice quality combined with flat interfaces in our Fe/Cr superlattices. However, our CEMS results (next section) indicate some diffusion of Cr atoms into the Fe layers, as shown below.

Local environment of Fe atoms

Fe/Ag multilayers

In order to obtain information on the atomic environment of the Fe atoms in the Fe/Ag multilayers, we have performed ^{57}Fe conversion-electron Mössbauer spectroscopy (CEMS) at room temperature (RT). The measured CEMS spectra are shown in Figure 2(a) for the Fe/Ag multilayer and

in Figure 2(b) for the the Fe/Cr multilayer. The interface samples are further labeled as (i) and the center samples as (ii).

The spectrum of the Fe/Ag center sample is characterized by a nuclear Zeeman-split sextet with narrow Lorentzian lines (linewidth (FWHM) $\Gamma = 0.31$ mm/s), typical for a unique ^{57}Fe lattice site. The hyperfine parameters obtained from a least-squares fit of the data are given in Table SI (see Supplemental Material, SM). The Mössbauer parameters of the Fe/Ag center sample are in good agreement with the hyperfine parameters measured at room temperature with our Mössbauer spectrometer on a bcc (α-) Fe calibration foil (hyperfine field $B_{hf} = 33.0$ T, isomer shift $\delta = 0.0$ mm/s, $\Gamma = 0.27$ mm/s). We may conclude that ^{57}Fe probe-layer atoms in the center of the Fe films, which are a distance of 4 ML Fe away from the Fe/Ag interface, have a bcc-Fe-type of local environment and do not sense any measurable influence from Ag atoms in the neighboring Ag(001) layers. Based on this observation, we consider Fe-Ag long-range chemical intermixing in these multilayers as negligible. Negligible Fe-Ag interdiffusion is supported by the fact that the Fe-Ag system is known to be immiscible in the bulk [46], and that the relatively high preparation temperature (160 °C) of our multilayers favors Fe-Ag chemical segregation.

Clearly, the Fe layers in the Fe/Ag multilayer (center) are ferromagnetically ordered at room temperature, and are *not* superparamagnetic, as the appearance of the magnetically-split sextet in Fig. 2(a)(ii) demonstrates. (Superparamagnetism would result in a central singlet or doublet feature which, however, is absent in Fig. 2(a)(ii)). Furthermore, the line intensity ratio (or spectral area ratio) of line #2 (or line #5) and line #3 (or line #4) (counted from left to right) is measured to be $x = I_2/I_3 = I_5/I_4 = 3.5$. Use of the relation $\langle\Theta\rangle = \arccos([(4-x)/(4+x)]^{1/2})$ (Ref. 47) provides a value for the average Fe spin direction (average spin canting angle $\langle\Theta\rangle$) between the direction of the incident γ-ray (or film normal direction) and the Fe spin direction of $\langle\Theta\rangle = 75°$. This demonstrates that in average the Fe magnetic moments in the center of the Fe layers are tilted by 75° away from the film normal direction, i.e., they are preferentially oriented in the film plane.

The CEM spectrum of the Fe/Ag interface sample [Fig. 2(a)(i)] is different from that of the center sample [Fig. 2(a)(ii)]. The former also consists of an apparent Zeeman sextet, but the apparent outer lines #1 and #6 are clearly non-Lorentzian (they are asymmetric towards the inner sides). This asymmetry reflects the influence of interfacial Ag atoms on the hyperfine properties of the interfacial ^{57}Fe probe atoms. Therefore, the spectrum had to be analyzed in terms of two different sextet components: First, sextet #1, which causes the apparent line asymmetry, implying a static distribution of hyperfine fields, $P(B_{hf})$, as shown on the right-hand side of Fig. 2(a)(i); $P(B_{hf})$ is caused by the interaction of interfacial ^{57}Fe-probe layer atoms with interfacial Ag atoms. Second, a sextet with sharp Lorentzian lines, originating from ^{57}Fe-probe layer atoms that are not affected by interfacial Ag atoms and are located farther away from the interface. The hyperfine parameters for the interface Fe/Ag multilayer, obtained from least-squares fitting, are given in Table SI (see Ref. 39). Within error margins, B_{hf} and δ of the sharp sextet in Fig. 2(a)(i) are in agreement with the corresponding values for

bulk bcc Fe. This demonstrates that the majority of the ^{57}Fe atoms in the probe layer (i.e., 74 %, as obtained from the relative spectral area of the sharp sextet) experience an undisturbed bcc-Fe environment, while only 26 % of the ^{57}Fe atoms are in contact with Ag interface atoms.

It is well known that Ag near-neighbor atoms (relative to the case of α-Fe at room temperature) reduce the magnitude of the hyperfine field B_{hf} (at room temperature) and increase the isomer shift δ of ^{57}Fe atoms [47]. If the nominally 0.7-ML thick ^{57}Fe(001)-probe layer were grown perfectly flat on a flat Ag(001) layer, we would expect that all ^{57}Fe probe-layer atoms (100 %) are in direct contact with interfacial Ag atoms. This is not the case, however, as we measure that only 26 % of the ^{57}Fe atoms in the probe layer sense Ag atoms. This corresponds to an equivalent of only ~ 0.2 ML of ^{57}Fe atoms in the probe layer. The majority (74 %) of the ^{57}Fe-probe layer atoms (equivalent to ~ 0.5 ML of ^{57}Fe in the probe layer) are *not* in contact with Ag interface atoms. We may conclude that the majority of the ^{57}Fe atoms of the probe layer reside in the volume of bcc-Fe-type islands, the latter having a smaller surface-to-volume ratio than an ideally flat Fe atomic layer. Thus, the concept of island growth of our films, inferred from small-angle X-ray reflectivity measurements (Fig. S2, see Ref. 39) is qualitatively confirmed by CEMS. As mentioned above, very likely Fe-Ag intermixing plays only a minor role, even at the ^{57}Fe/Ag interface, since severe intermixing would increase the fraction of Ag neighboring atoms for ^{57}Fe atoms in the probe layer, and keep this fraction high (near 100 %), in contrast to our measured fraction of only 26 %.

The appearance of the magnetically-split sextets in Fig. 2(a)(i) (measured in zero applied magnetic field) proves that the Fe layers in the Fe/Ag interface sample are ferromagnetic and *not* superparamagnetic. Also, this is true for the center sample, Fig. 2(a)(ii). Obviously, the Fe island size in both samples is large enough (or the islands interact with each other) to prevent superparamagnetism at room temperature. Furthermore, the average Fe spin orientation in the interface sample is also preferentially in the film plane (Table SI, see Ref. 39).

Fe/Cr multilayers

Figure 2(b) displays CEM spectra taken at room temperature from the interface ^{57}Fe probe layer (i) and the center ^{57}Fe probe layer (ii) in the Fe/Cr multilayers. The spectrum of the center sample is characterized by a dominant Zeeman-split sextet with narrow Lorentzian lines, and a weak sextet with broadened outer lines typical for a distribution of hyperfine fields P(Bhf), as shown on the right-hand side. The Mössbauer parameters of the sharp sextet (Table SI, Ref. 39) are similar to those of bcc Fe. Thus, the sharp sextet originates from ^{57}Fe probe-layer atoms in the center of the 8-ML thick ^{56}Fe layer that do not experience interaction with Cr atoms. On the other hand, the weak P(B_{hf}) distribution should arise because a fraction of ^{57}Fe probe-layer atoms (41 % according to Table SI, Ref. 39) in the center of the Fe film sense Cr atoms in their local environment. This reveals that some Cr diffusion into the neighboring ^{56}Fe layers over a distance of 4 ML Fe occurs, which reaches some ^{57}Fe atoms

even in the center of the ^{56}Fe layers. This behavior is different from that in the center Fe/Ag multilayer, where no Ag diffusion into the center of the Fe film could be detected [see the sharp bcc-Fe-like sextet in Fig. 2(a)(ii)].

It is striking that the CEM spectrum of the Fe/Cr interface sample in Fig. 2(b)(i) looks very different from the corresponding spectrum of the Fe/Ag interface sample [Fig. 2(a)(i)]. The Fe/Cr interface spectrum was fitted with a sharp sextet (of 21 % in relative spectral area) and a distribution of hyperfine fields $P(B_{hf})$ (of 79 % in relative spectral area), the latter displayed in Fig. 2(b)(i) on the right-hand side. The very wide $P(B_{hf})$ distribution is characterized by several peaks, i.e., several distinct ^{57}Fe sites, as a result of the interaction with nearest and next-nearest Cr atoms in the alloyed Fe/Cr interfacial region [34,37,48-51]. Here, the average hyperfine field, $<B_{hf}>$, averaged over the distribution $P(B_{hf})$, is found to be 22.2 T. It is interesting that small angle X-ray reflectometry (see Ref. [34], Fig. 2) (which gives information on the mesoscopic scale) of our epitaxial Fe(001)/Cr(001) multilayer center and interface samples provides evidence of the high-quality superlattice structure implying sharp interfaces on a mesoscopic scale, while CEMS (providing information on the atomic scale) demonstrates that the interfaces in the same Fe/Cr multilayer samples are not sharp but chemically intermixed [34,37,48-51].Quantitatively, we measure that out of the 0.7-ML thick ^{57}Fe probe layer at the Fe/Cr interface an equivalent of 0.55 ML of ^{57}Fe sense Cr atoms, whilst only 0.15 ML of ^{57}Fe do not interact with Cr atoms and have a bcc-Fe-type of local surroundings.

The wide distribution of hyperfine fields in the Fe/Cr case (as, e.g., for our Fe/Cr interface sample) occurs in random bulk Fe-Cr alloys [52] and near intermixed Fe/Cr interfaces [34,37,48-51]. It is the existence of ^{57}Fe atoms with a distribution of local (atomic) magnetic moments [34,51] and with different local (atomic) environments near the alloyed Fe/Cr interface that leads to the apparent satellite lines in the Mössbauer spectra [Fig. 2(b)(i)] and, accordingly, to the wide $P(B_{hf})$ distribution. Nearest (nn) and next-nearest (nnn) neighboring Cr atoms (relative to a ^{57}Fe atom) in random bulk Fe-Cr alloys induce a large hyperfine-field change (decrease) of $\Delta B_{hf}(nn) = -3.02$ to -3.21 T per nn Cr atom and $\Delta B_{hf}(nnn) = -2.29$ to -2.16 T per nnn Cr atom, respectively (as compared to the 'undisturbed' pure bcc-Fe hyperfine field B_{hf} of 33.0 T for the ^{57}Fe atom at room temperature), resulting in the wide $P(B_{hf})$ distribution [52]. A similar situation is found in the Fe/Cr interface region due to diffusion of Cr atoms into the Fe layers [34,37,48-51]. For the Fe/Ag(001) system, the hyperfine distribution P(Bhf) reported in the literature [47] is much narrower than in the Fe/Cr case due to very small or negligible interdiffusion of Fe/Ag. Furthermore, the magnitude of the (effective) $\Delta B_{hf}(nn) \sim -1.6$ T per nn Ag atom for Fe/Ag(001), as estimated for the "interface site 1" with $B_{hf} = 26.7$ T and with 4-nn Ag atoms in Ref. 47 appears to be about a factor of 2 smaller than the magnitude of $\Delta B_{hf}(nn) = -3.02$ T per nn Cr atom for Fe/Cr.

C. Nuclear resonant inelastic X-ray scattering (NRIXS)

^{57}Fe NRIXS measurements were performed at room temperature at the undulator beamline 3-ID at the Advanced Photon Source, Argonne National Laboratory. The method of NRIXS is selective to the ^{57}Fe resonant isotope and measures the phonon excitation probability, as described in Refs. [53-56]. This provides the Fe-partial phonon (vibrational) density of states (VDOS) rather directly with a minimum of modeling [57]. The monochromatized synchrotron radiation was incident onto the thin-film multilayers under a grazing angle of ≈ 4°. The synchrotron-beam energy was scanned around the resonant energy of the ^{57}Fe nucleus (14.413 keV) with an energy resolution ΔE of 2.3 meV for the Fe/Cr superlattices and 0.9 meV for the Fe/Ag multilayers. For each sample, the instrumental resolution function was determined by measuring the nuclear forward scattering intensity. The collection times were ~ 10 – 24 h per spectrum. The evaluation of the NRIXS spectra was performed using the PHOENIX software by W. Sturhahn [57].

We like to make a remark on the angular emission probability of phonons, as the synchrotron X-ray beam with wave vector $\mathbf{k_0}$ impinges on the multilayer surface at grazing incidence in our experiment. The NRIXS signal is sensitive to the projection $<\mathbf{k_0}\bullet\mathbf{u}>$ of the displacement vector **u** of the Fe atom on the photon wave vector $\mathbf{k_0}$ [58], i.e., the Fe-specific VDOS measured by NRIXS are projections of the real Fe-VDOS onto the X-ray beam direction $\mathbf{k_0}$. This fact could become important in the case of anisotropic solids [59], such as the present Fe(001)/Ag(001) interfaces which might show vibrational anisotropy by its structure. In NRIXS, only such phonons (of mode j) can be excited whose displacement vectors **u** (or polarization vectors $\mathbf{e}_j(\mathbf{q})$) possess a component parallel to the beam direction $\mathbf{k}_0$. More specifically, the incoherent cross section (probability W(E)) of nuclear resonance absorption for a particular phonon energy E and phonon momentum vector **q** is given by [59]:

$$W(E) \sim |\mathbf{s} \bullet \mathbf{e}_j(\mathbf{q})|^2 \qquad \text{Eq.(1)}$$

where $\mathbf{e}_j(\mathbf{q})$ is the polarization vector of vibrations for the Fe atom in the phonon mode j [58,59], and $\mathbf{s} = \mathbf{k_0}/|\mathbf{k_0}|$ is the unit vector in the photon momentum direction. This implies a scaling of W(E) with $\cos^2(\Theta)$, with Θ being the angle between the phonon polarization vector $\mathbf{e}_j(\mathbf{q})$ and the X-ray direction **s.** Here, the index j refers to longitudinal acoustic (LA) or transverse acoustic (TA) phonon modes. Eq. (1) tells us that NRIXS should be able to detect any phonons whose polarization vector has a component along the incident X-ray direction, which is nearly in the film plane (off by ~ 4° only) in our set-up. For a polycrystalline sample, in the average $|\mathbf{s} \bullet \mathbf{e}_j(\mathbf{q})|^2$ = constant and the VDOS is independent of the angle θ [8, 59]. Phonons with $\mathbf{e}_j(\mathbf{q})$ perpendicular to the incident X-ray direction are not sensed by NRIXS . In this sense, the phonon DOS obtained by NRIXS on our epitaxial (anisotropic) multilayers are Fe-partial as well as directionally 'projected' Fe-VDOS. This is in contrast to the computed Fe-VDOS (see section IV.B.(a)), which are atom-projected (Fe-partial) total VDOS and not direction-projected VDOS. Therefore, some differences between the theoretical and

experimental Fe-VDOS might be expected. However, we anticipate observing some general trends by comparing the experimental and the computed non-projected Fe-VDOS. For comparison, we have computed also Fe-projected (projected along the incident X-ray beam direction) VDOS for Fe/Ag and Fe/Cr, as described in section IV.B.(c).

III. Theoretical Methods

Density functional theory (DFT) [60,61] calculations were performed to investigate the formation of Fe/Ag and Fe/Cr multilayers within the projector augmented wave (PAW) method [62] implemented in the Vienna *ab initio* simulation package (VASP) [63,64]. The schematic models for Fe/Ag and Fe/Cr multilayers together with their interfaces are presented in Figure 1(c) and (d), respectively. The model Fe/Ag (Fe/Cr) multilayer system consists of 8 ML Fe and 8 ML Ag (Cr) to mimic the experimental thickness of the corresponding multilayer system (see section II.A). We use a (2x2) plane unit cell. Thus, each model system is made of 32 Fe and 32 Ag (Cr) atoms. The Fe/Ag interface was modeled by creating epitaxial 45° rotated fcc(100) layers on top of bcc(100) layers. Such an interface enables almost a perfect lattice match between Fe and Ag layers reducing surface tension in the interface, whose (bulk) experimental lattice constants (2.87 Å and 4.09 Å, respectively) differ by a factor of 1.43 (1.466 in case of theoretical lattice constants: 2.83 Å and 4.15 Å, respectively) . Similarly, the Fe/Cr interface was modeled by epitaxial layers of bcc(100). In this case, both elements have almost identical (experimental) lattice constants (2.87 Å and 2.88 Å, respectively). Moreover, in order to further reduce any interfacial tension present, we performed a variable cell minimization of these model structures. In the technique, supercell shapes and sizes can be changed using the supercell stress. Such structures have negligible stress. The resulting supercells have the following dimensions: 5.68 Å x 5.68 Å x 22.6 Å for Fe/Cr and 5.73 Å x 5.73 Å x 28.6 Å for Fe/Ag. Also, the entire multilayers in the supercells are fully relaxed until the forces on atoms reduce to below 0.01 eV/Å. We use a 6 x 6 x 1 k-mesh for sampling the Brillouin zone and a Fermi-level smearing of 0.2 eV. Exchange-correlation energy is included in the calculation using the Perdew-Burke-Enzerhof functional [65]. The cut-off energy for plane-waves was 340 eV. The threshold for electronic energy convergence was set to 1×10^{-5} eV ($1x10^{-8}$ eV for phonon calculations), and that for structural optimization to $< 1\times10^{-2}$ eV/Å. These settings allow accurate calculations of forces and energies, which are needed for calculations of phonons.

For calculation of the phonon density of states we employed the PHONOPY code [66,67]. The phonon dispersion curves are calculated using the direct method [68], in which vibrational frequencies and eigenvectors can be obtained by diagonalization of the dynamical matrix which contains the force constants calculated from the forces on atoms obtained by displacing individual atoms. We use VASP

to obtain the forces. The supercell size used in the calculation is 2x2x2. The resulting supercells have the following dimensions: 11.36 Å x 11.36 Å x 45.2 Å for Fe/Cr and 11.46 Å x 11.46 Å x 57.2 Å for Fe/Ag. The theoretical phonon DOS of section IV.B.(a) (below) are only atom-projected (partial) VDOS and not direction-projected (partial) VDOS (see Section II.C). However, results of calculations of the direction-projected partial Fe-VDOS for Fe/Ag and Fe/Cr using PHONOPY will be reported in section IV.B.(c) below. The angular-momentum-decomposed electronic local density of states (DOS) of the multilayers was calculated by projecting the wave function into the PAW sphere at each Ag (or Cr) atom. Bader charge analysis [69,70] was also performed to calculate charge redistribution in the interface. The magnetic moment of each atom is obtained by integrating spin-up minus spin-down charge densities within each Bader volume.

IV. Results and Discussion

A. Experiment

Figure 3 exhibits the Fe-projected/Fe-partial VDOS, g(E), measured by ^{57}Fe NRIXS at room temperature on the Fe/Ag (a) and Fe/Cr (b) multilayers containing ^{57}Fe probe layers. Also, the VDOS of bulk Fe is shown for comparison. The NRIXS raw data are displayed in Figure S3 (for Fe/Ag) and Figure S4 (for Fe/Cr) in Ref. 39.

The VDOS of the center Fe layer in Figure 3(a) shows similarities to the VDOS of bulk Fe: the latter is characterized by the sharp longitudinal-acoustic (LA) phonon peak at 36 meV and by the two resolved transverse-acoustic (TA) phonon peaks at ~ 23 meV and ~ 27 meV [71]. However, as compared to the LA peak height of ~ 220 $eV^{-1}at.vol.^{-1}$ of bulk Fe, the LA peak in the center Fe layer appears to be reduced to ~ 150 $eV^{-1}at.vol.^{-1}$, thus approaching the TA peak height of ~ 150 $eV^{-1}at.vol.^{-1}$ in the center Fe layer of the Fe/Ag multilayer. It is also interesting that the low-energy part of the VDOS below ~ 20 meV is enhanced for the Fe/Ag center layer. In Fig. 3 (a), the cut-off energies of the center Fe layer and of bulk Fe are found to be about equal (~ 39 - 40 meV). For Fe/Ag, one can notice differences between the VDOS of the center Fe layer and of the interface Fe layer. Fig. 3 (a) reveals important features: (i) the LA-phonon peak for the interface is remarkably reduced to ~ 130 $eV^{-1}at.vol.^{-1}$ and simultaneously is shifted to lower energy (to ~ 33 meV); quantitatively, the ratio of the peak heights near 35 meV for the Fe/Ag interface layer to the center layer is found to be 0.87. (ii) the TA-phonon peaks for the interface become dominant and shift to lower energies, with a maximum at ~ 24 meV (and height ~ 160 $eV^{-1}at.vol.^{-1}$) and with a strong side peak at ~ 20 meV (and height ~ 145 $eV^{-1}at.vol.^{-1}$); (iii) for the interface, a strong enhancement of g(E) exists in the low-energy region (E < ~ 20 meV), which is much stronger than that for the center layer. This observation implies that the phonon features experience a distinct red shift in the interface Fe layer of Fe/Ag as compared to

the center Fe layer of bulk bcc Fe. Looking at the cut-off-energy of ~ 39 – 40 meV in the VDOS in Fig. 3 (a), it remains the same for the center Fe and interface Fe layer within error margins.

As for the Fe/Cr multilayer, Fig. 3 (b), the center Fe layer exhibits a VDOS very similar to that of bulk Fe, showing a dominant sharp LA-phonon peak at 35 meV (and height ~ 175 eV^{-1}at.vol.$^{-1}$) and the two TA-phonon peaks at 27 meV (height ~ 155 eV^{-1}at.vol.$^{-1}$) and 23 meV (height ~ 150 eV^{-1}at.vol.$^{-1}$). As compared to the LA peak of bulk Fe height (~ 220 eV^{-1}at.vol.$^{-1}$), obviously the LA-peak height is reduced in the center Fe layer, contrary to the positions and the heights of the TA-phonon peaks, which are about similar to those of bulk Fe. The situation changes for the interface Fe layer in Fe/Cr, as can be seen in Fig. 3(b). Although the position of the sharp LA-phonon peak at 35 meV in the interface Fe layer remains the same as in the center Fe layer, the LA peak height of the interface is reduced to a value of 150 eV^{-1}at.vol.$^{-1}$. The experimental ratio of g(E) near ~ 35 meV for the interface to the center Fe layer is found to be 0.91, which is somewhat larger than the same ratio for Fe/Ag. Simultaneously, the two TA-phonon peaks become badly resolved at the Fe/Cr interface. The TA-phonon feature increases in peak height to a value of 170 eV^{-1}at.vol.$^{-1}$ at 23 meV, and the higher-energy TA peak shifts from 27 meV (in the center Fe layer) to ~ 25 meV in the interface Fe layer. Also, it is interesting that for Fe/Cr in the low-energy regime below ~ 18 meV no measurable difference exists in g(E) of the interface Fe, the center Fe layer and bulk bcc Fe, Figure 3(b), in striking contrast to the case of the Fe/Ag interface layer, for which an overall strong red shift of the VDOS is observed at low phonon energies (Fig. 3(a)). The typical features in the VDOS of Fe/Ag and Fe/Cr center and interface Fe layers, respectively, are summarized in Table I.

A qualitatively similar reduction of the LA-phonon peak height at ~ 35 meV combined with an enhancement of the low-energy part of the VDOS below ~ 18 meV, as in the present Fe/Ag samples, was previously observed in nanoscale polycrystalline $[^{57}Fe/Ag(40Å)]_{15}$ multilayers containing homogeneous ^{57}Fe layers 1.5 to 4 nm in thickness when the ^{57}Fe layer thickness decreases down to 1.5 nm [21]. This effect was attributed to Fe phonon confinement and interface localization due to the VDOS energy mismatch between of Fe and Ag. These phenomena were found to be nearly absent in polycrystalline $[^{57}Fe/Cr(40Å)]_{15}$ multilayers containing thin homogeneous ^{57}Fe layers.

The NRIXS results allow the calculation of vibrational thermodynamic quantities. These quantities are given in Table II. The corresponding equations for the calculations, relating g(E) and the thermodynamic quantities, can be found in the literature [5-8,58]. One can notice in Table II that in the Fe/Ag multilayer system the Lamb-Mössbauer factor, f_{LM}, and the mean atomic force constant are significantly reduced, and the vibrational entropy is enhanced at the Fe/Ag interface as compared to the center Fe layer. This is in contrast to the Fe/Cr multilayer, where no significant change in these quantities between the interface and the center layer is observed. According to Table II, bulk bcc Fe has the largest f_{LM} and the largest mean atomic force constant, but the smallest vibrational entropy and smallest vibrational specific heat.

Interestingly, qualitatively similar modifications in the high-energy and low-energy part of the Fe-VDOS of the Fe/Ag multilayers from the Fe bulk properties were observed by NRIXS in a single epitaxial bcc-Fe layer on W(110) [72] deposited and studied in ultrahigh vacuum. Moreover, phonon damping in polycrystalline bcc-Fe thin films deposited onto a Pd buffer layer, again with qualitatively similar modifications of the Fe-VDOS, was reported in Ref. 73. These results are in line with our present observation on Fe/Ag, since both bulk W and Pd are 'soft' materials from the phonon point of view, with lower Debye temperatures (θ_D) of 400 K and 274 K, respectively, as compared to θ_D(Fe) = 470 K of bulk bcc-Fe [16].

B. Theory

(a) Phonon density of states, confinement and localization

Figure 4 shows the calculated element-projected phonon density of states (VDOS) of (a) Fe/Ag and (b) Fe/Cr multilayers, respectively. Here, only the VDOS for the interface and center layers are displayed (meaning the center of the individual Fe or Ag (Cr) films). The computation described in this section provides the directionally-unprojected partial VDOS. (For the direction-projected partial Fe-VDOS, see section IV.B.(c) below).

The VDOS for the Fe interface layer in the Fe/Ag system shows unique features and remarkable changes as compared to the more bulk-like VDOS of the center Fe layer, Figure 4(a). The VDOS of the Fe interface in Fe/Ag has several distinct features and is far from the typical appearance of the bulk Fe phonon density of states, and even resembles more the VDOS of the Ag interface layer, but is shifted to higher energy. The signature peak of bulk bcc Fe (essentially the longitudinal-acoustic (LA) phonon peak at 34.5 meV in the computation) is completely diminished for interfacial Fe, combined with a remarkable increase of the low-energy phonon peaks. Eigenvector analysis (Figure 5(a)) shows that this mode is a mixed mode confined in Fe layers (mostly in-plane vibrations with small cross-plane displacements). On the other hand, the VDOS of the center Fe layer Fig. 4(a), is almost similar to the VDOS of bulk Fe [71] and is characterized by the dominant (LA phonon) peak at 35.6 meV and by the two peaks of transverse-acoustic (TA) phonons at 23.0 meV (T1) and 27.0 meV (T2) [71]. These features indicate that (contrary to the Fe interface layers) the Fe phonons in the Fe center layers do not sense a significant perturbation by the Fe/Ag interface.

The calculated Ag-partial VDOS, Fig. 4(a), shows that the VDOS of the Ag center layer is characterized by a dominant peak at 19.3 meV (the LA phonon peak) and peaks at 11.2 meV and 7.2 meV (TA phonon peaks). These features are in good agreement with the VDOS of bulk Ag [71]. For the Ag interface layer, the LA phonon peak at 19.3 meV is strongly reduced, and at low energy (8.8 meV) a new dominant and broad feature appears. Our observation for Ag in Fig. 4(a) implies that an

overall hardening of the Ag phonons occurs going from the center Ag layer to the interface Ag layer in the Fe/Ag multilayer. One can also see in Figure 4(a) that the calculated cut-off energy of ~ 23 meV of the Ag partial VDOS in the center Ag layer is smaller than the cut-off energy of about 29 meV for the interface Ag layer.

Not as drastic as the case of Fe/Ag but the VDOS of the Fe interface in the Fe/Cr system shows similar trends and shares some common features, i.e, a decrease (but no shift) of the LA-phonon peak (now at 35.6 meV) as compared to the VDOS of the center Fe layer and a smearing of the two TA phonon peaks resulting in a new peak at 24 ~ 27 meV, Figure 4(b). For the center Fe layer, the LA-phonon peak (at 39.6 meV) is rather sharp, and the two TA-phonon peaks at 24.4 meV and 27.3 meV are resolved, but they show an asymmetry in peak heights. The Cr-projected VDOS of the Cr layers shows softening: the main peak at 39.9 meV (LA phonons) shifts to 36.7 meV, in going from the center Cr layer to the interface Cr layer, and the two TA modes at 27.3 meV and 33.0 meV are smeared but remain resolved.

Figure 4(c) exhibits the calculated layer-resolved Fe-partial VDOS for the Fe/Ag multilayer. One can observe a systematic trend: while Fe layer 4 (center layer) shows a VDOS rather similar to that of bulk Fe with the distinct LA phonon peak at ~ 35 meV and TA phonon peaks at ~27 and ~23 meV, the dominant feature at ~35 meV shifts to lower energy and decreases in peak height the closer the Fe layer approaches the interface. For instance, for Fe layers 3 and 2 the LA phonon peak shifts to ~ 34.3 meV and ~ 34.0 meV, respectively. For Fe layer 1 (the interface layer), the LA phonon peak typical for bulk Fe nearly disappears. From Fig. 4(c), the theoretical peak-height ratio in g(E) near ~ 35 meV for the interface (Fe layer 1) to the center Fe layer (Fe layer 4) is equal to 0.103 only, which is far off from the corresponding experimental ratio of 0.87 for Fe/Ag. It is interesting, however, that this theoretical ratio jumps to ~ 0.80 and thus nearly approaches the experimental value of 0.87, if the ratio is calculated for the subinterface (Fe layer 2) to the center layer (Fe layer 4) in Fig. 4(c).

Combined with the reduction of the LA phonon peak, drastic changes occur in the features characteristic for the lower-energy Fe phonons as one approaches the Fe/Ag interface: in Fe layers 3 and 2, the two TA phonon peaks around ~ 23 meV and ~ 27 meV are still observable, but their relative peak heights are strongly modified, and simultaneously a low-energy feature near ~ 15 meV emerges. These effects at low phonon energies are most drastic for the Fe layer 1 (the interface Fe layer), for which the feature at ~ 15 meV becomes dominant at the expense of the higher energy part of the VDOS. Note that the energies of the enhanced Fe phonons below ~25 meV in the VDOS of Fe layers overlap with those in the VDOS of Ag layers, Fig. 4(a), indicating that the Fe phonons couple with the Ag ones at the corresponding energies. For example, the eigenvector analysis of the 15-meV mode demonstrates that it is in fact coupled with the vibrations of center Ag layers, Figure 5(b). It is thus clear that the low-energy enhancement is caused by softening of Fe phonons due to coupling with Ag

phonons. One can also notice in Fig. 4(c) that the calculated cut-off energy of ~ 39 meV of the Fe-projected VDOS is independent of the layer distance to the Fe/Ag interface. Moreover, Fe phonons above ~29 meV have no counterpart in the VDOS of Ag, Fig. 4(a), indicating their confinement in the Fe layers. The layer-resolved eigenvector analysis of each Fe layer for the 35-meV mode, as shown in Fig. 5(a) shows that in going from the Fe center layer to the Fe interface layer, the vibrational amplitude abruptly decreases nearly to zero since the Ag layers cannot accommodate their high frequency vibration owing to the large mass ratio of ~2 for Ag/Fe. Such a phenomenon is not expected for Fe/Cr with a mass ratio of ~ 1.

Furthermore, there are "localized" phonon modes, whose vibrations are confined in a single (either Fe or Ag) atomic layer, which can be either an interfacial or non-interfacial layer. To identify localized modes, we use the normalized inverse participation ratio (NIPR) [3], which is defined for eigenvectors $u_{i\alpha}$ of a phonon k, as

$$NIPR[k] = N\sum_{i=1}^{N}(\sum_{\alpha=1}^{3} u_{i\alpha}^{2}[k])^{2},$$

where N is the number of atoms. The larger the *NIPR*, the more localized the phonon and *N/NIPR* represents the number of participating atoms in the motion of phonon k. Figure 6(a) presents the calculated NIPR for Fe/Ag phonon modes. Clearly, phonons with low energy, especially, below 15.2 meV, are more localized than those with high energy above 23 meV. In our Fe/Ag multilayer system, each layer consists of 4 Fe (or Ag) atoms. Thus, if N/NIPR $\leq$ 6, it may be regarded as localized in a single layer. Fig. 6(a) shows that all of the localized modes in single-layer have energy smaller than 15.2 meV. All localized modes turn out to be cross-plane modes (wave vector pointing along the [001] direction perpendicular to the film plane) with in-plane vibrations. About 58 % (42%) of the localized modes are Ag (Fe) modes, and, importantly, 88 % of the localized (Fe and Ag) modes are localized *at the interface.* Such a mode is shown in Figure 6(b).

We may compare our DFT-based interfacial VDOS in the present Fe/Ag multilayer with g(E) at the Fe/Ag interface of Fe nanoclusters deposited on a Ag(001) substrate, as obtained from molecular dynamics calculations [74]. The Fe/Ag interface of the Fe nanoclusters was defined by Fe atoms with at least one Ag atom in the first two atomic neighbor shells. The calculated g(E) at the interface in these Fe nanoclusters on Ag(001) looks drastically different from the corresponding experimental and DFT-computed VDOS in the present Fe/Ag(001) multilayers. The calculated interfacial g(E) of the Fe nanoclusters was found to extend up to very high phonon energies (up to ~ 60 meV), has a very broad maximum at ~ 25 meV, and exhibits a low-energy enhancement below ~ 15 meV relative to g(E) of bulk bcc Fe. The center region of the Fe nanoclusters was calculated to have a bulk-like VDOS, except that the ~ 36-meV peak is reduced. This effect has been previously ascribed to phonon damping[75,76], and may be due to ~ 36-meV phonon confinement in the center region of the Fe nanoclusters[74]. The ~ 36-meV peak of bulk bcc Fe or of the center region in the nanoclusters is

practically absent at the Fe/Ag interface of the nanoclusters, and instead a very broad shoulder evolves. We speculate that the distinct differences observed between the molecular-dynamics calculated interfacial g(E) of the Fe nanoclusters on Ag(001) and the experimental and DFT-computed interfacial VDOS in the present Fe/Ag(001) multilayers may be caused by strong interfacial stress/strain in the Fe nanoclusters.

(b) Electronic structure

In order to understand the causes of such remarkably different results for the vibrational dynamics of interfaces in Fe/Ag and Fe/Cr multilayers, we first analyze the geometric structure of our model systems shown in Fig. 1(c) and 1(d). The calculated average interlayer distances for central Fe-Fe and Ag-Ag layers are 1.401 Å and 2.136 Å, respectively, in close agreement with a previous theoretical study (1.38 and 2.07 Å, respectively [77]). Our calculated distance for the Fe-Ag interface separation [Fig. 1(c)] is 1.899 Å, which is ~36% longer than the average central Fe-Fe interlayer distance (1.401 Å), but ~11% shorter than the average center Ag-Ag interlayer distance (2.135 Å). Our Fe-Ag interface separation distance (1.899 Å) is slightly larger than the one in the previous study (1.85 Å) [77]. The Fe-Cr interface separation (1.380 Å) shows a similar trend [(Fig. 1(d)]. We find next that the calculated electronic structure also shows strong chemical interaction at the Fe/Ag and Fe/Cr interfaces. For Fe/Ag, the calculated magnetic moment $\mu_{Fe,int}$ of 2.8 μ_B of the Fe interfacial atoms, Figure 7(a), is found to be substantially higher than that of the other Fe atoms ($\mu_{Fe,center}$ = 2.3 μ_B), including the center Fe layers in agreement with the previous study (2.82 μ_B) [77]. This is the result of electronic charge transfer from Fe to Ag atoms at the interface, as shown in Figure 7(b): ~ 0.15 electrons are transferred from a Fe interface atom to an Ag interface atom. The situation is quite different for the Fe/Cr multilayer. Here, the calculated magnetic moment of an interface Fe atom of $\mu_{Fe,int}$ = 1.9 μ_B appears to be reduced relative to $\mu_{Fe,center}$ = 2.3 μ_B of the center Fe layer, Fig. 8(a), which is the result of charge transfer of 0.32 electrons from a Cr atom to a Fe atom at the interface, Fig. 8(b).

The transferred electrons induce strong electrostatic coupling between Fe/Ag interface layers resulting in a hardening of the Ag-Fe bond at the interface. This hardening can be seen in the VDOS of the Fe/Ag interface. In Fig. 4(c), the Fe signature peak in the VDOS near 35 meV slightly decreases in energy going from the center towards the interface (35.3 meV for 4th layer, 34.2 meV for the 3rd layer, 34.0 meV for the 2nd layer). However, at the interface the energy slightly increases again to 34.2 meV. This increase may be attributed to the strong coupling between Fe and Ag interface atoms, although Fe-Fe coupling gets weaker going towards the interface, as electron charge density redistributes from the center to the interface.

The calculated Fe-projected layer-resolved electronic density of states, D(E), are presented in Figure 8(a) for Fe/Ag and in Figure 8(b) for Fe/Cr. We find that a strong perturbation in the electronic structure occurs only directly at the Fe/Ag interface. More spin-up and less spin-down states are

occupied in such a way that Fe donates more spin-down electrons to Ag, but receives less spin-up electrons from Ag. Since Ag at the interface has an almost fully occupied d-band (note: the d-band of an isolated Ag atom is full), Ag can receive only spin-down electrons and becomes completely non-spin polarized. (Note in Fig. 7(a) that interfacial Ag has no magnetic moment).

Note that completely new peaks in D(E) (labeled A for spin-up (↑) and B for spin-down (↓) states) appear for the Fe/Ag interface [Fig. 8(a)], which does not occur either for the inner Fe layers or for the Fe/Cr interface, Fig. 8(b). This is the reason for the existence of a large predicted electronic spin polarization $P = [D_{\uparrow}(E_F) - D_{\downarrow}(E_F)]/[D_{\uparrow}(E_F) + D_{\downarrow}(E_F)]$ at the Fermi energy, $E_{F,}$ for the Fe(001)/Ag(001) interface: P = - 0.79 (or - 79 %) is obtained from Fig. 8(a). Normally, such a large perturbation in the electronic structure of the Fe/Ag interface would affect the dynamic stability of the interface, causing softening in the VDOS. Indeed, in our calculated phonon dispersion curves (Fig. S5, Ref. 39) there are negative modes at the Γ point associated with the interface, suggesting a long-ranged instability of the modeled Fe/Ag interface.

Another aspect to be considered regarding the instability of the Fe/Ag and Fe/Cr multilayers is the occurrence of large charge transfer at the interface (0.32 electrons for Fe/Cr and 0.15 electrons for Fe/Ag). In general, this would put the Fe multilayers into a recurring sandwich structure of alternating positive and negative layers. If the net electric dipole moment of such structures is not zero, such multilayers are inherently unstable (Figs. S5 and S6, in Ref. 39). In order to become stabilized, the interface would reconstruct [78]. Interestingly, our experiments indicate that only ~26 % of Fe atoms (or ~ 0.2 ML of the ~ 0.7-ML thick ^{57}Fe interfacial probe layer) at the interface are in contact with Ag atoms and possibly ^{57}Fe island are formed at the interface, whereas there is much stronger intermixing in the Fe/Cr interfacial region (79 % of the ^{57}Fe probe layers sense Cr atoms, see section II.B), combined with approximate layer-by-layer growth. In the non-flat Fe/Ag and highly-intermixed Fe/Cr interfaces in the experiment such a polarized interface as seen in our theoretical model may not result. If so, the difference in interface structure may be the primary cause for the described discrepancies in our experiment and theoretical results, particularly the drastic reduction of the VDOS of the 35 meV mode for the Fe/Ag interface. We also would like to note that in a previous study [79] the reconstruction (island formation and intermixing) of the perfectly flat Fe/Ag interface was attributed to interface strain due to lattice mismatch and (or) surface energy mismatch between Ag and Fe. A similar explanation was given for the reconstruction of Fe/Au multilayers [32]. Thus, the actual cause for the instability of the perfect interface can be of elastic and electrostatic origin.

Another factor for the discrepancy can be that the experimental Fe-specific VDOS represents the Fe-VDOS projected to the direction of the grazing-incident X-ray beam, as has been outlined in section II.C, while the DFT calculated VDOS of this section comprises the total (unprojected) Fe-partial VDOS. The experimental Fe-VDOS might not completely include the full contribution from

the cross-plane phonon modes due to the experimental setup. Due to the asymmetry of the multilayer structure of our sample, such cross-plane phonons are expected to be different from in-plane phonons, in particular at the anisotropic interfacial layers of Fe/Ag. Thus, they may be not easily picked up and could be partially missing in the experimental Fe-VDOS. We will theoretically investigate this question in section IV.B.(c) below.

(c) Direction-projected Fe-partial VDOS

As we have mentioned in section II.C on NRIXS, in the case of anisotropic solids, Eq.(1) might become important, which projects the phonon polarization vector $\mathbf{e}_j(\mathbf{q})$ for a phonon mode j onto the vector **s** of the incident x-ray direction [59]. Eq.(1) then leads to the Fe-*projected* vibrational (phonon) DOS. In particular, the Fe/Ag(001) interfaces in the Fe/Ag multilayers appears to be highly anisotropic from the phonon point of view, much more than the Fe/Cr interfaces. Thus, the calculation of the Fe-projected VDOS under this geometrical condition is required for the comparison with the experimental result. We have computed the Fe-projected VDOS of Fe/Ag and Fe/Cr with the projection along the incident x-ray beam, i.e., with the beam 4° above the in-plane [100] direction. (In the following we will label this geometry as '[100]-projected' or simply 'projected').

In Figure 9 we provide the directionally-projected partial Fe-VDOS and compare them with the experimental Fe-VDOS. The projection vector **s** = (0.9976, 0.0, -0.0697) in Cartesian coordinates was in accord with the direction of the grazing-incident X-ray beam in the experiment. Figure 9(a) displays the unprojected (black line) and projected (blue line) calculated VDOS of the Fe/Ag(001) center layer, and the experimental VDOS (red line) [from Fig. 3(a)] of the Fe/Ag center sample. First of all, the unprojected and projected VDOS are virtually identical for the center Fe layer. This is expected because the bulk-like center layer is locally more or less symmetric, and the vibrational anisotropy is lost. But as it comes to the subinterface layer (Fe layer 2 in Fig. 1(c)), due to increased asymmetry, substantial differences are expected. This is exactly seen in Figure 9(b), which displays the unprojected and projected calculated Fe-VDOS of the Fe/Ag(001) subinterface layer (black and blue lines, respectively). Going further, Figure 9(c) displays the unprojected and projected calculated Fe-VDOS of the Fe/Ag(001) interface layer (black line and blue line, respectively), and the experimental Fe-VDOS [from Fig. 3(a)] of the Fe/Ag interface sample (red line). The projected VDOS shows substantial change from the unprojected VDOS in the entire energy range shown, and a consistent trend is that the projected VDOS shows enhanced features at lower energy and reduced features at higher phonon energy. These differences are related to the vibrational anisotropy of the interface Fe layers in the Fe/Ag(001) multilayer and is a consequence of Eq.(1).

When we compare the calculated VDOS with the experimental VDOS of the center Fe layer (Fig. 9(a)), they are in good agreement with the exception of the height of the signature peak at ~35 meV. Moreover, we observe an overall shift to lower energy (red-shift) of the experimental Fe-VDOS

relative to the computed VDOS (lattice softening), very likely due to the finite measurement temperature (room temperature) and thermal expansion in the experiment (the DFT-based calculations are representative of T = 0 K). However, when it comes to the interface VDOS, the calculated Fe-projected VDOS of Fe/Ag multilayers agrees only qualitatively with experiment. The change in the calculated Fe-projected VDOS at the interface is much more drastic than the change in the corresponding measured VDOS. Such a large softening of modes in the calculated Fe-VDOS of the Fe/Ag interface may suggest that the assumed interface geometry used in our theory would undergo reconstruction (not considered in our model) owing to instability of the Fe/Ag interface. In fact, a softening for the Fe/Ag interface is also observed in the experiment (Fig. 3(a)), although it is not as dramatic as in the calculation (Fig. 4(a)). While the experimental Fe-VDOS deviates strongly from the calculated unprojected and projected g(E) in case of the interface Fe layer, the experimental g(E) carries features (peaks) of the Fe subsurface layer, although it is shifted to lower phonon energy relative to g(E) of the subinterface. The experimental interfacial VDOS is seen to be located in energy between the calculated (ideally sharp) Fe/Ag interface (Fe layer 1) and the subinterface (Fe layer 2). Interestingly, the least-square fit of the experimental VDOS in Fig. 9(d) can be obtained by mixing 29% of the projected interface VDOS and 71% of the projected subinterface VDOS. This suggests that the experimental VDOS is indeed closer to the theoretical subinterface VDOS, particularly at high phonon energy, but comes with substantial contribution from the interface VDOS at low energy. This observation leads us to conclude that the Fe local atomic environment near the interface in our experimental interface Fe/Ag sample is in between that of the ideally flat interface and that of the ideally flat subinterface. This conclusion agrees qualitatively with the concept of a slightly intermixed Fe/Ag interface in the experimental sample, as inferred from CEMS (see section II.B).

For the Fe/Cr(001) multilayer, the direction-projected and unprojected Fe-VDOS (see Figures S7(a) and S7(b) in Ref. 39) hardly show any significant difference. In comparison with experiment, an excellent agreement among the unprojected and projected calculated Fe-VDOS and the experimental Fe-VDOS is found for the Fe center layer (Fig. S7(a), Ref. 39), but for the interface Fe layer (Figure S7(b), Ref. 39) the calculated Fe-VDOS shows a much stronger phonon peak around 25 meV than the experimental VDOS.

V. Conclusions

Isotope-selective ^{57}Fe nuclear resonant inelastic x-ray scattering (NRIXS) measurements and atomic-layer resolved density functional theory (DFT) calculations were used to investigate the effect of interfaces on the vibrational density of states (VDOS) of (001)-oriented nanoscale Fe/Ag and Fe/Cr multilayers. The calculations were performed for the case of unprojected (total) partial VDOS and for the case of direction-projected Fe-partial VDOS, with the projection along the direction of the incident

X-ray beam. For Fe/Ag multilayers, the experimental and theoretical results demonstrate high-energy phonon confinement in the Fe layers and lower-energy phonon localization at the Fe/Ag interface due to the energy mismatch between Ag and Fe phonons. For the Fe center layer in Fe/Ag, the computed and experimental Fe-VDOS are in fair agreement and show features of the VDOS of bcc Fe. At the Fe/Ag interface, however, the high-energy longitudinal-acoustic (LA) phonon mode of Fe near ~ 35 meV is strongly suppressed in the calculations, and the low-energy part of the VDOS below ~ 20 meV is drastically enhanced, as compared to the Fe-specific VDOS in the center Fe layers or in bulk Fe. These effects (seen in the calculations) are much less pronounced in the experimental interfacial Fe-VDOS, very likely due to an imperfect Fe/Ag growth and atomic intermixing at the Fe/Ag interface. The computed and experimental Fe-VDOS for the Fe center layer in Fe/Cr are in good agreement and show features of the VDOS of bcc Fe. On the other hand, the Fe-VDOS of the Fe/Cr interface is characterized by some reduction of the ~ 35-meV peak and an enhancement of the VDOS near 24 meV in both experiment and theory, with the 24-meV peak enhancement being more significant in the calculations. Overall, the experimental and calculated Fe-projected/Fe-partial VDOS for the Fe/Cr multilayers are in good agreement. Distinct differences were observed between the calculated unprojected Fe-VDOS and the direction-projected Fe-VDOS for the Fe/Ag(001) interface (but not for the Fe/Cr(001) interface) as a result of its strong vibrational anisotropy/asymmetry.

Our calculations revealed that both Fe/Ag and Fe/Cr atoms at the interface are strongly coupled chemically as indicated by a large charge transfer (0.15 and 0.32 electrons per layer, respectively). However, such a strong charge transfer causes the interface to become polarized, potentially leading to electrostatic instability. It is the large interfacial charge transfer combined with the large atomic mass ratio of Ag/Fe that results in the remarkable modification of the Fe-projected VDOS at the Fe/Ag interface. The experimentally obtained Fe-partial vibrational thermodynamic properties of the Fe/Ag interface are found to be different from those in the center of the Fe layer or from bulk bcc Fe.

We believe that our present findings are generally valid for other nanoscale metallic multilayer systems with large interfacial charge transfer and large atomic mass ratio. Our observation of a strongly modified VDOS at the interface in a multilayer system have impact on the atomistic understanding of such physical properties of phononic systems, where the interfacial phonon density of states (VDOS) enters as a decisive factor, such as, e.g., in phonon transport properties of multilayers and thermocrystals [4, 9, 10].

Acknowledgments

The authors are grateful to Ulrich von Hörsten (University of Duisburg-Essen) for preparing and characterizing the multilayer samples and for his outstanding technical assistance. Theoretical calculations (SH and TSR) were supported by U.S. DOE under grant DE-FG02-07ER46354. The

experimental work (BRC) was partially funded by the US National Science Foundation (NSF-DMR 1207065). This research used resources of the Advanced Photon Source, a U.S. Department of Energy (DOE) Office of Science User Facility operated for the DOE Office of Science by Argonne National Laboratory under contract no. DE-AC02-06CH11357.

REFERENCES

1. Srivastava, G. P., *The Physics of Phonons* (Adam Hilger, Bristol, Philadelphia, New York, 1990).
2. T. Gorishnyy, C. K. Ullal, M. Maldovan, G. Fytas, and E. L. Thomas, Phys. Rev. Lett. **94**, 115501 (2005).
3. L. Yang, N. Yang, and B. Li, Sci. Rep. **3**, 1143 (2013).
4. H. Mizuno, S. Mossa, and J.-L. Barrat, Sci. Rep. **5**, 14116 (2015).
5. Grimvall, G., *Thermophysical Properties of Materials (Selected Topics in Solid State Physics) Vol. 18 (North-Holland, Amsterdam, 1986)*
6. B. Fultz,Prog. Mater. Sci. **55**, 247 (2010).
7. S. Stankov, M. Miglierini, A. I. Chumakov, I. Sergueev, Y. Z. Yue, B. Sepiol, P. Svec, L. Hu, and R. Rüffer, Phys. Rev. B **82**, 144301 (2010).
8. M. Y. Hu, T. S. Toellner, N. Dauphas, E. E. Alp, and J. Zhao, Phys. Rev. B 87, 064301 (2013).
9. M. Maldovan, Nature **503**, 209 (2013).
10. M. Maldovan, Phys. Rev. Lett. **110**, 025902 (2013).
11. Z. Li, S. Tan, E. Bozorg-Grayeli, T. Kodama, M. Asheghi, G. Delgado, M. Panzer, A. Pokrovsky, D. Wack, and K. E. Goodson, Nano Lett. **12**, 3121 (2012).
12. R. Venkatasubramanian, E. Slivola, T. Colpitts, and B. O'Quinn, Nature **413**, 597 (2001).
13. T. C. Harman, P. J. Taylor, M. P. Walsh, and B. E. LaForge, Science **297**, 2229 (2002).
14. D. Vashaee and A. Shakouri, Phys. Rev. Lett. **92**, 106103 (2004).
15. A. Balandin and K. L. Wang, J. Appl. Phys. **84**, 6149 (1998).
16. C. Kittel, *Introduction to Solid State Physics*, 5th edition,(J. Wiley & Sons, New York, London, Sidney, Toronto, 1976) p. 126 .
17. R. M. Costescu, D. G. Cahill, F. H. Fabreguette, Z. A. Sechrist, and S. M. George, Science **303**, 989 (2004).
18. E. Dechaumphai, D. Lu, J. J. Kan, J. Moon, E. E. Fullerton, Z. Liu, and R. Chen, Nano Lett. **14**, 2448 (2014.
19. E. T. Swartz and R. O. Pohl, Rev. Mod. Phys. **61**, 605 (1989).
20. P. Reddy, K. Castelino, and A. Majumdar, Appl. Phys. Lett. **87**, 211908 (2005).
21. B. Roldan Cuenya, W. Keune, R. Peters, E. Schuster, B. Sahoo, U. von Hörsten, W. Sturhahn, J. Zhao, T. S. Toellner, E. E. Alp, and S. D. Bader, Phys. Rev. B **77**, 165410 (2008).
22. S. Tan et al., Nature Mater. **12**, 634 (2013).
23. J. J. Lee et al., Nature **515**, 245 (2014).
24. B. Jusserand and M. Cardona, in *Light Scattering in Solids V,* Topics in Applied Physics*, edited by M. Cardona and G. Güntherodt (Springer, Berlin, 1989), p. 49*.
25. C. Colvard, R. Merlin, M. V. Klein, and A. C. Gossard, Phys. Rev. Lett. **45**, 298 (1980).
26. A. K. Sood, J. Menendez, M. Cardona, and K. Ploog, Phys. Rev. Lett. **54**, 2111 (1985).
27. A. K. Sood, J. Menendez, M. Cardona, and K. Ploog, Phys. Rev. Lett. **54**, 2115 (1985). M.

28. M. Grimsditch, J. E. Mattson, C. H. Sowers, S. D. Bader, and M. J. Peters, Phys. Rev. Lett. **77**, 2025 (1996).
29. P. Baumgart, B. Hillebrands, R. Mock, G. Güntherodt, A. Boufelfel, and C. M. Falco, Phys. Rev. B **34**, 9004 (1986).
30. J. A. Bell, W. R. Bennett, R. Zanoni, G. I. Stegeman, C. M. Falco, and F. Nizzoli, Phys. Rev. B **35**, 4127 (1987).
31. J. R. Dutcher, S. Lee, J. Kim, G. I. Stegeman, and C. M. Falco, Phys. Rev. Lett. 65, 1231 (1990).
32. M. Sternik, K. Parlinski, and J. Korecki, Phys. Rev. B **74**, 195405 (2006).
33. T. Ruckert, W. Keune, W. Sturhahn, M. Y. Hu, J. P. Sutter, T. S. Toellner, and E. E. Alp, Hyperfine Interact. **126**, 363 (2000).
34. V. M. Uzdin, W. Keune, H. Schrör, and M. Walterfang, Phys. Rev. B **63**, 104407 (2001).
35. W. Sturhahn, R. Roehlsberger, E. E. Alp, T. Ruckert, H. Schrör, and W. Keune, J. Magn. Magn. Mater. **198-199**, 590 (1999).
36. Y. Kozono, M. Komuro, S. Narishige, M. Hanazono, and Y. Sugita, J. Appl. Phys. **63**, 3470 (1988). Y., et al., *Structures and magnetic properties of Fe/Ag multilayer films prepared by sputtering and ultrahigh-vacuum depositions.* Journal of Applied Physics, 1988. **63**(8): p. 3470-3472.
37. J. Landes, Ch. Sauer, R. A. Brand, W. Zinn, S. Mantl, and Zs. Kajcsos, J. Magn. Magn. Mater. **86**, 71 (1990).

38. W. Keune and W. Sturhahn, Hyperfine Interact. **123-124**, 847 (1999).
39. See Supplemental Material at [URL will be inserted by publisher] , which includes Refs. [36,40-45], for supporting information on crystallographic orientation, multilayer periodicity, Mössbauer parameters, NRIXS raw data, phonon dispersion curves, and comparison of calculated and experimental phonon DOS of Fe/Cr multilayers.
40. B. T. Jonker and G. A. Prinz, Surf. Sci. **172**, L568 (1986).
41. N. C. Koon, B. T. Jonker, F. A. Volkening, J. J. Krebs, and G. A. Prinz, Phys. Rev. Lett. **59**, 2463 (1987).
42. M. Stampanoni, A. Vaterlaus, M. Aeschlimann, and F. Meier, Phys. Rev. Lett. **59**, 2483 (1987).
43. D. E. Bürgler, C. M. Schmidt, D. M. Schaller, F. Meisinger, R. Hofer, and H.-J. Güntherodt, Phys. Rev. B **56**, 4149 (1997).
44. B. E. Warren, *X-ray Diffraction* (Addison-Wesley, Reading, Mass., 1989) pp. 370-371.
45. A. Schreyer, J. F. Ankner, Th. Zeidler, H. Zabel, M. Schäfer, J. A. Wolf, P. Grünberg, and C. F. Majkrzak, Phys. Rev. B 52, 16066 (1995).
46. T. B. Massalski, *Binary Alloy Phase Diagrams* (American Society for Metals, Metals Park, Ohio, 1987)
47. P. J. Schurer, Z. Celinski, and B. Heinrich, Phys. Rev. B **48**, 2577 (1993).

48. F. Klinkhammer, Ch. Sauer, E. Yu. Tsymbal, S. Handschuh, Q. Leng, and W. Zinn, J. Magn. Magn. Mater. **161**, 49 (1996).
49. M. Kubik, T. Slezak, M. Przybylski, W. Karas, and J. Korecki, Vacuum **63**, 337 (2001).
50. V. Uzdin, W. Keune, and M. Walterfang, J. Magn. Magn. Mater. **240**, 504 (2002).
51. V. M. Uzdin and W. Keune, J. Phys.: Condens. Matter **19**, 136201 (2007).
52. S. M. Dubiel and J. Zukrowski, J. Magn. Magn. Mater. **23**, 214 (1981).
53. M. Seto, Y. Yoda, S. Kikuta, X. W. Zhang, and M. Ando, Phys. Rev. Lett. **74**, 3828 (1995).
54. W. Sturhahn, T. S. Toellner, E. E. Alp, X. Zhang, M. Ando, Y. Yoda, S. Kikuta, M. Seto, C. W. Kimball, and B. Dabrowski, Phys. Rev. Lett. **74**, 3832 (1995).
55. A. I. Chumakov, R. Rüffer, H. Grünsteudel, H. F. Grünsteudel, G. Grubel, J. Metge, and H. A. Goodwin, Europhys. Lett. **30**, 427 (1995). .
56. A. I. Chumakov and W. Sturhahn, Hyperfine Interact. **123-124**, 781 (1999).
57. W. Sturhahn, Hyperfine Interact. **125**, 149 (2000).

58. R. Röhlsberger, *Nuclear Condensed Matter Physics with Synchrotron Radiation (Springer, Berlin, 2004).*
59. V. G. Kohn, A. I. Chumakov, and R. Rüffer, Phys. Rev. B **58**, 8437 (1998)
60. P. Hohenberg and W. Kohn, Phys. Rev. **136**, B864 (1964).
61. W. Kohn and L. J. Sham, Phys. Rev. **140**, A1133 (1965).
62. P. E. Blöchl, Phys. Rev. B **50**, 17953 (1994).
63. G. Kresse and J. Furthmüller, Phys. Rev. B **54**, 11169 (1996).
64. G. Kresse and J. Hafner, Phys. Rev. B **47**, 558 (1993).
65. J. P. Perdew, K. Burke, and M. Ernzerhof, Phys. Rev. Lett. **77**, 3865 (1996). Erratum Phys. Rev. Lett. **78**, 1396 (1997).
66. A. Togo and I. Tanaka, Scr. Mater. **108**, 1 (2015).
67. *This code can be downloadable from https://atztogo.github.io/phonopy/index.html.*
68. K. Parlinski, AIP Conf. Proc. **479**, 121 (1999).
69. R. Bader, *Atoms in Molecules: A Quantum Theory* (Oxford University Press, New York, 1990).
70. G. Henkelman, A. Arnaldsson, and H. Jónsson, Comput. Mater. Sci. **36,** 354 (2006).
71. P. H. Dederichs, H. Schober, and D. J. Sellmyer, in *Metals: Phonon States, Electron States and Fermi Surfaces*, Landolt-Börnstein, New Series, Group III, Vol. 13, edited by K.-H. Hellwege and J. L. Olsen (Springer, Heidelberg, 1981).

72. S. Stankov, R. Röhlsberger, T. Slezak, M. Sladecek, B. Sepiol, G. Vogl, A. I. Chumakov, R. Rüffer, N. Spiridis, J. Lazewski, K. Parlinski, and J. Korecki, Phys. Rev. Lett. 99, 185501 (2007).

73. R. Röhlsberger, W. Sturhahn, T. S. Toellner, K. W. Quast, P. Hession, M. Hu, J. Sutter, and E. E.Alp, J. Appl. Phys. **86**, 584 (1999).

74. B. Roldan Cuenya, A. Naitabdi, J. Croy, W. Sturhahn, J. Y. Zhao, E. E. Alp, R. Meyer, D. Sudfeld, E. Schuster, and W. Keune, Phys. Rev. B **76**, 195422 (2007).
75. B. Fultz, C. C. Ahn, E. E. Alp, W. Sturhahn, and T. S. Toellner, Phys. Rev. Lett. **79**, 937 (1997).
76. H. Frase, B. Fultz, and J. Robertson, Phys. Rev B 57, 898 (1998).
77. S. Lu, Q.-M. Hu, M. P. J. Punkkinen, B. Johansson, and L. Vitos, Phys. Rev. B **87**, 224104 (2013).
78. P. W. Tasker, J. Phys. C: Solid State Physics **12**, 4977 (1997).
79. P. J. Schurer, Z. Celinski, and B. Heinrich, Phys. Rev. B **51**, 2506 (1995).

Table I. Longitudinal-acoustic (LA) phonon peak height in g(E) near ~ 35 meV**,** relative change Δg(E) (relative to g(E) at 36 meV of bulk Fe), and LA phonon peak energy, as obtained by ^{57}Fe NRIXS. The data marked by * are taken from Ref. [21] for Fe/Ag and Fe/Cr multilayers with homogeneous ^{57}Fe layers.

Sample	g(E) peak height (eV^{-1}at.vol.$^{-1}$)	change Δg(E) (%)	LA peak energy (meV)
Fe/Ag interface	~ 130	40.9	~ 33
Fe/Ag center	~ 150	31.8	~ 34
$[Fe(8nm)/Ag(4nm)]_{15}$*	162	26.4	34.9
Fe/Cr interface	~ 150	31.8	~ 35
Fe/Cr center	~ 175	20.4	~ 35
$[Fe(8nm)/Cr(4nm]_{15}$*	185	15.9	35.2
Bulk bcc Fe	~ 220	0	36.0

Table II: Fe-specific vibrational thermodynamic quantities of the Fe/Ag (Fe/Cr) center sample and Fe/Ag (Fe/Cr) interface sample at room temperature, extracted from the experimental phonon density of states in Fig. 3. Lamb-Mössbauer factor (f_{LM}), kinetic energy (K), vibrational entropy (S_V) at constant volume, vibrational specific heat (C_V) and mean atomic force constant. The data marked with * correspond to polycrystalline references samples discussed in Ref. [21].

Sample	**Lamb-Mössbauer factor, f_{LM}**	**Kinetic Energy, K (meV/ atom)**	**Vibrational entropy, S_v (k_B/atom)**	**Vibrational specific heat, C_v (k_B/atom)**	**Mean atomic force constant (N/m)**
Fe/Ag center	0.773 ± 0.003	42.3 ± 0.5	3.24 ± 0.02	2.74 ± 0.02	161 ± 6
Fe/Ag interface	0.734 ± 0.003	42.0 ± 0.5	3.51 ± 0.03	2.76 ± 0.02	151 ± 6
[^{57}Fe(8 nm)/Ag(4 nm)]$_{15}$ multilayer*	0.765 ± 0.0006	42.1 ± 0.2	3.279 ± 0.009	2.752 ± 0.009	152 ± 2
[^{57}Fe(1.5 nm)/Ag(4 nm)]$_{15}$ multilayer*	0.7147 ± 0.0007	41.8 ± 0.2	3.46 ± 0.01	2.77 ± 0.01	140 ± 2
Fe/Cr center	0.785 ± 0.003	42.5 ± 0.3	3.19 ± 0.02	2.74 ± 0.02	162 ± 5
FeCr interface	0.787 ± 0.003	42.3 ± 0.3	3.20 ± 0.02	2.74 ± 0.02	159 ± 5
[^{57}Fe(8 nm)/Cr(4 nm)]$_{15}$ multilayer*	0.7812 ± 0.004	42.4 ± 0.1	3.203 ± 0.006	2.735 ± 0.006	166 ± 1
[^{57}Fe(2 nm)/Cr(4 nm)]$_{15}$ multilayer*	0.7827 ± 0.0007	42.3 ± 0.2	3.23 ± 0.01	2.740 ± 0.01	160 ± 2
Bulk bcc-Fe	0.7951 ± 0.0006	42.54 ± 0.06	3.133 ± 0.009	2.723 ± 0.009	175 ± 2

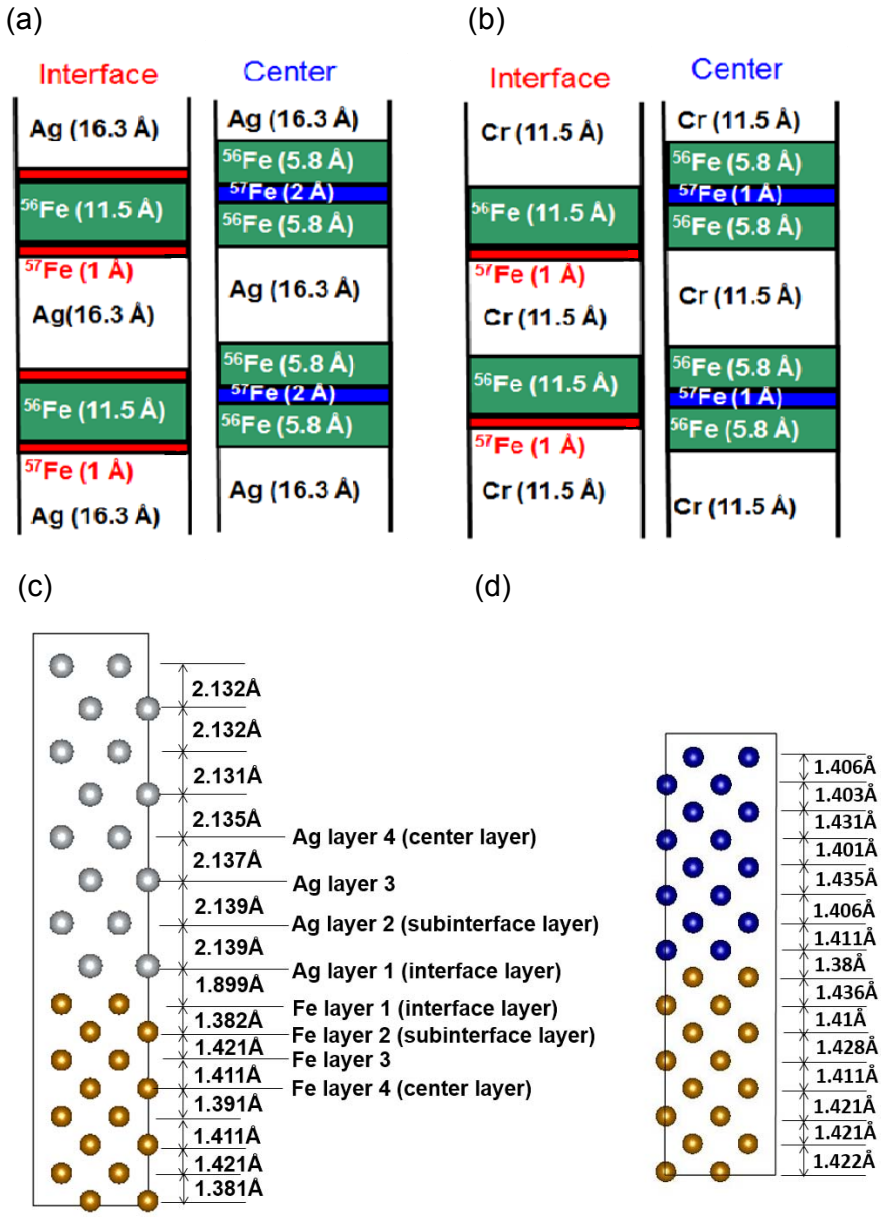

FIG. 1: (Color online) Schematic experimental (a),(b) and theoretical (c),(d) structural models of (a),(c) Fe/Ag and (b),(d) Fe/Cr multilayers. In the drawing of the experimental samples, the ^{57}Fe layers are plotted in red when they are located at the interface of Ag or Cr, and in blue when they are placed at the center of a ^{56}Fe layer. In the theoretical plots, the numbers indicate in-plane and out-of-plane atomic distances. Symbols: Ag atoms (silver), Fe atoms (gold), Cr atoms (blue).

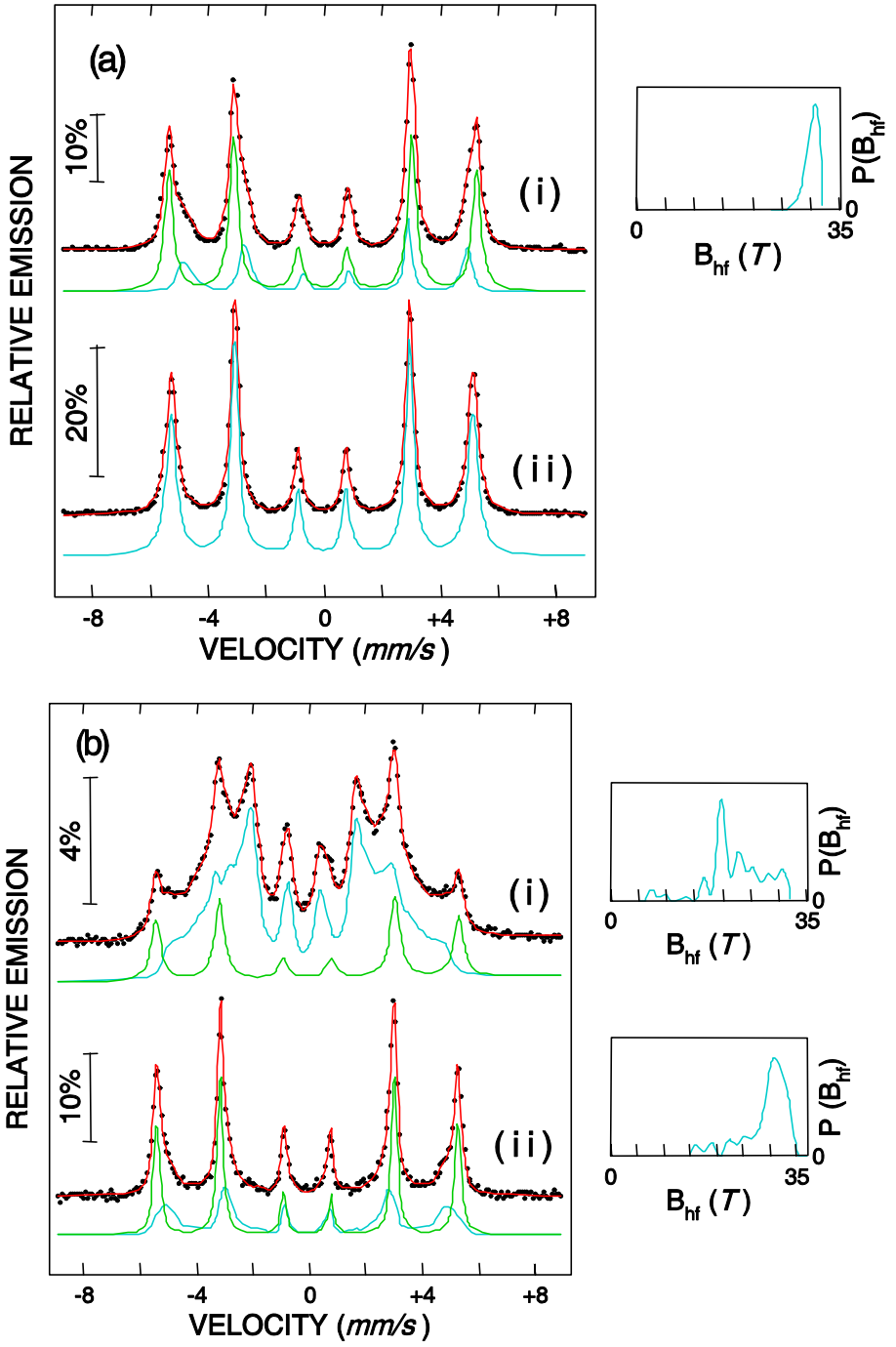

FIG. 2: (Color online) ^{57}Fe conversion-electron Mössbauer spectra (CEMS) taken at 25°C from (a) Fe/Ag, and (b) Fe/Cr multilayers: (i) "interface" and (ii) "center" samples. In (a)(ii), the data were fit with one sextet with sharp Lorentzian lines (blue line). In (a)(i), (b)(i) and (b)(ii), the data were least-squares fit with two spectral components: a sextet with sharp Lorentzian lines (green line), and a component (blue line) characterized by a distribution, $P(B_{hf})$, of hyperfine magnetic fields B_{hf} (shown in each case on the right-hand side). Red lines: fits to the data. The fit parameters obtained are shown in Table SI (Ref. 39).

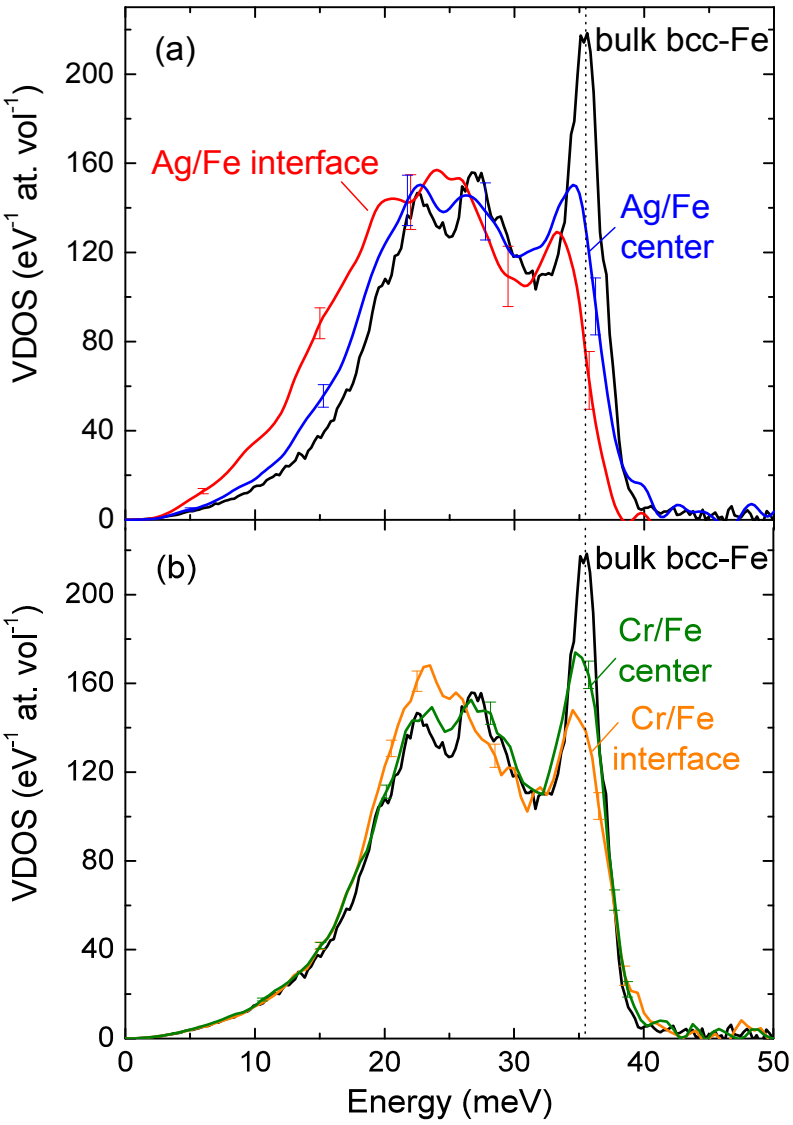

FIG. 3: (Color online) Fe-projected vibrational density of states (VDOS), g(E), obtained by ^{57}Fe NRIXS at room temperature for (a) Fe/Ag multilayers, and (b) Fe/Cr multilayers. All samples contain ultrathin ^{57}Fe probe layers either at the interface or in the center of the Fe layer. (a) Fe/Ag center layer (blue line) and interface layer (red line). (b) Fe/Cr center layer (green line) and interface layer (orange line). For comparison, also the VDOS of bulk bcc Fe at room temperature is shown (black lines), and the position of the LA peak near 36 meV is shown by the vertical dotted line. The energy resolution ΔE is 0.9 meV for Fe/Ag and 2.3 meV for Fe/Cr. Representative error bars are shown in (a) and (b).

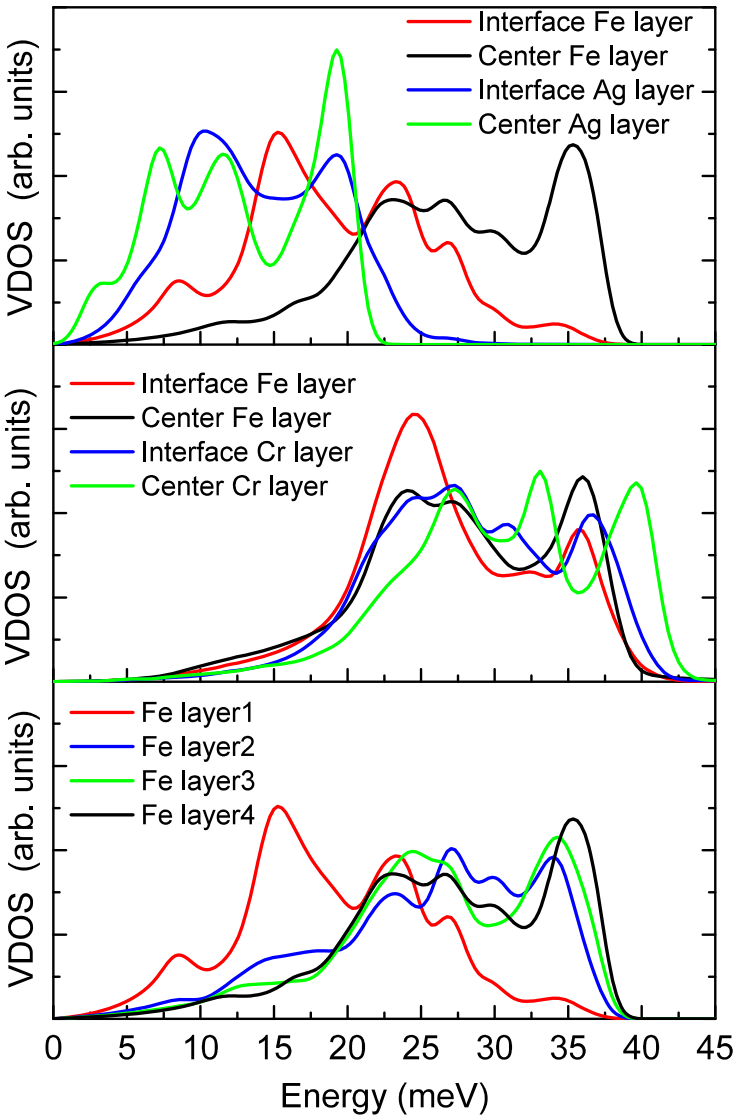

FIG. 4: (Color online) DFT-calculated element-projected (partial) phonon density of states (VDOS) for (a) Fe/Ag(001) and (b) for Fe/Cr(001) multilayers. Only the VDOS of the interfacial and center layers of Fe and Ag or Cr are shown. (c) Calculated layer-resolved Fe-projected VDOS for the Fe/Ag(001) multilayer. Layer 1 (red: interface Fe layer; layer 2 (blue): second Fe layer from the interface; layer 3 (green): third Fe layer from the interface; layer 4 (black): center Fe layer. A Fermi-level smearing of 0.2 eV was used in the DFT calculations.

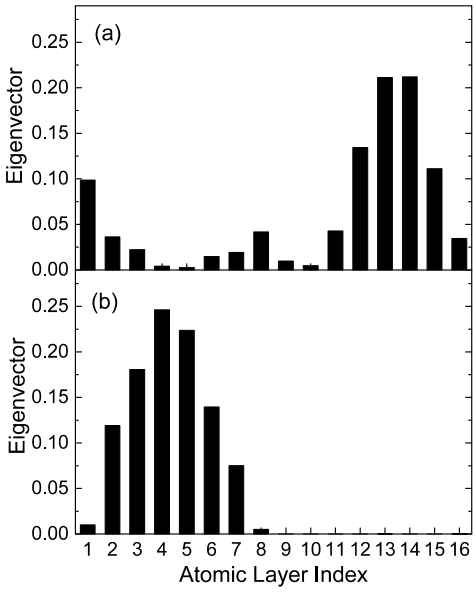

FIG. 5: (a) Eigenvector analysis of the calculated longitudinal-acoustic phonon mode at 35 meV versus the the atomic-layer number in the bilayer of the Fe(8ML)/Ag(8ML) multilayer. The vibrational amplitude (vertical scale, arb. units) is found to decrease abruptly nearly to zero at the Fe/Ag interface (Fe layers number 1 and 8) as compared to the center Fe layer (Fe layer number 4). This demonstrates confinement of the 35-meV mode in the Fe layer. (b) Eigenvector analysis of the calculated phonon mode at 15 meV versus the atomic-layer number in the bilayer of the Fe(8ML)/Ag(8ML) multilayer. The vibrational amplitude (vertical scale, arb. units) demonstrates that the 15-meV phonon mode of Fe is coupled with the 15-meV vibrations of center Ag layers.

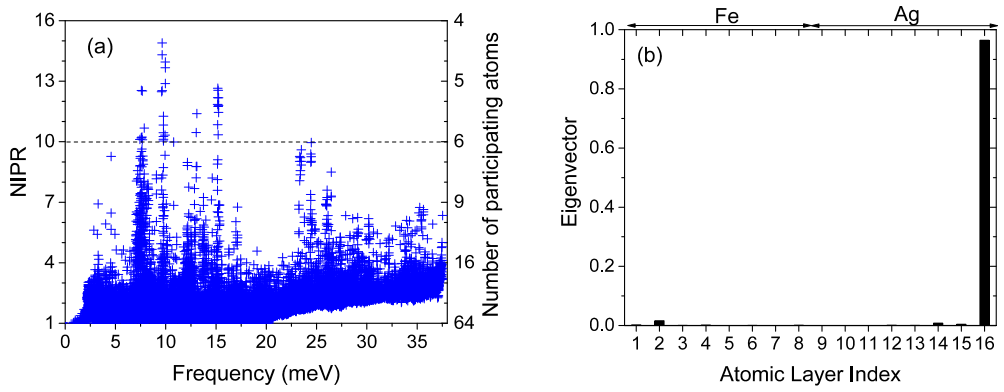

FIG. 6*:* (Color online) (a) The calculated NIPR spectrum of the Fe/Ag(001) multilayer system. The horizontal dashed line represents the condition that N/NIPR = 6. Phonons above the dashed line are considered as localized vibrations in a single layer; (b) The eigenvectors of atoms of the localized phonon mode at 9.6 meV with the highest NIPR value (14.9 in (a)). This mode is localized at the Ag interface layer.

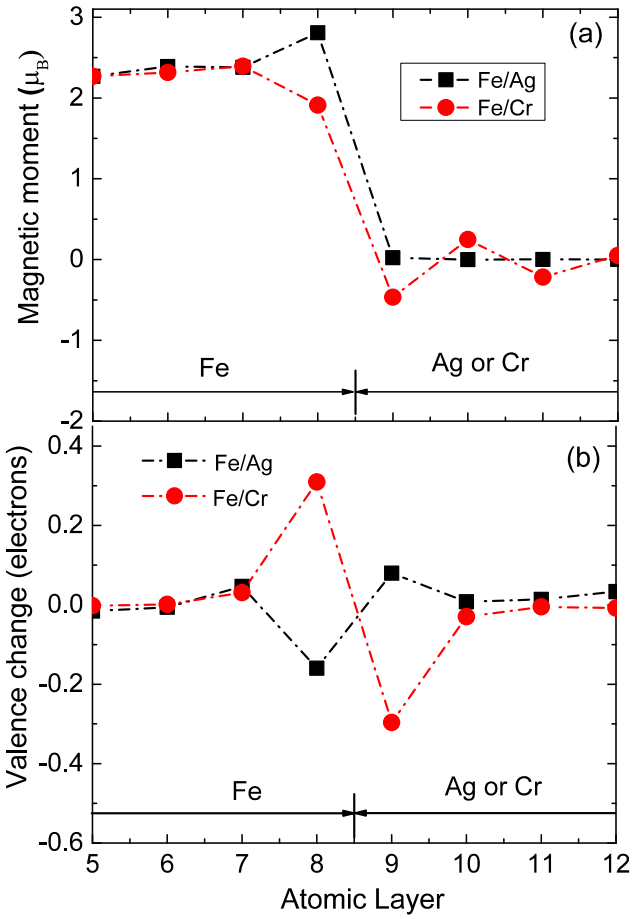

FIG. 7: (Color online) DFT-calculated layer-resolved (a) magnetic moments and (b) d-valence charge change along the film normal direction of Fe/Ag(001) and Fe/Cr(001) multilayers, respectively. In (b), the positive value means electron accumulation (or valence increase), and the negative value means electron depletion (or valence decrease). Layer index 1: center Ag (or Cr) layer; layer index 4: interface Ag (or Cr) layer; layer index 5: interface Fe layer; layer index 8: center Fe layer.

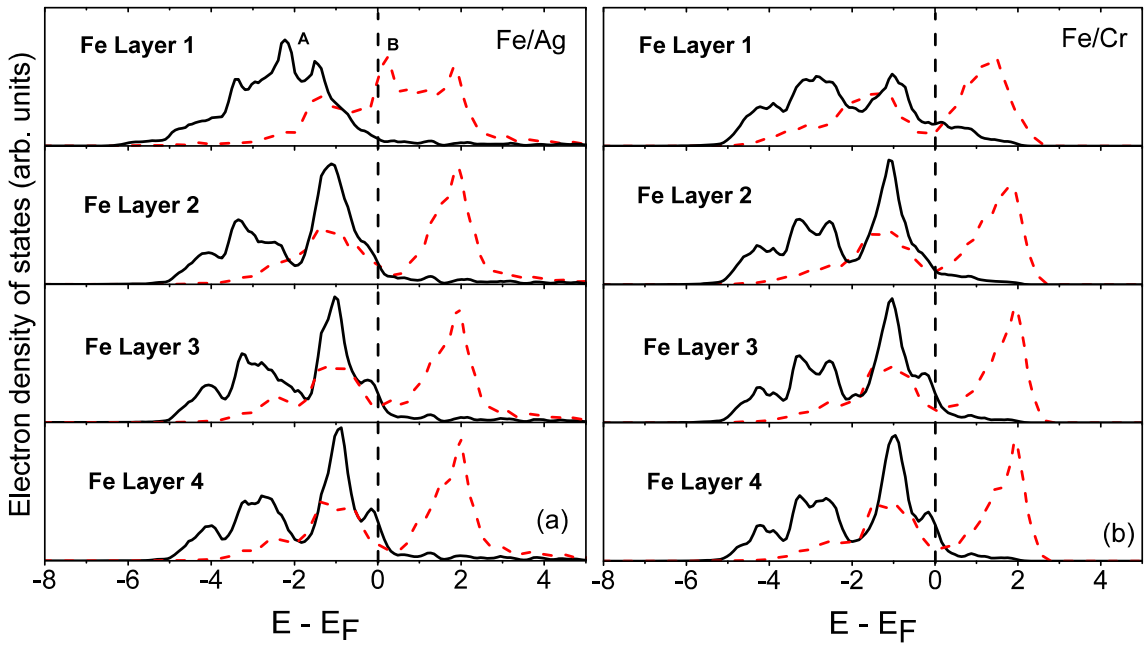

FIG. 8*:* (Color online) DFT-calculated layer- and spin-resolved electronic density of states, D(E), of the Fe layer in (a) Fe/Ag(001) multilayer and (b) Fe/Cr(001) multilayer. Fe layer 1 is located directly at the Fe/Ag or Fe/Cr interface, and Fe layer 4 is is the center layer in the Fe film. Fe layer 2 (Fe layer 3) is the second (third) Fe layer from the interface. Majority spins: black lines; minority spins: red dotted lines. (E_F = Fermi energy). A and B indicate peaks that exist only at the Fe/Ag interface.

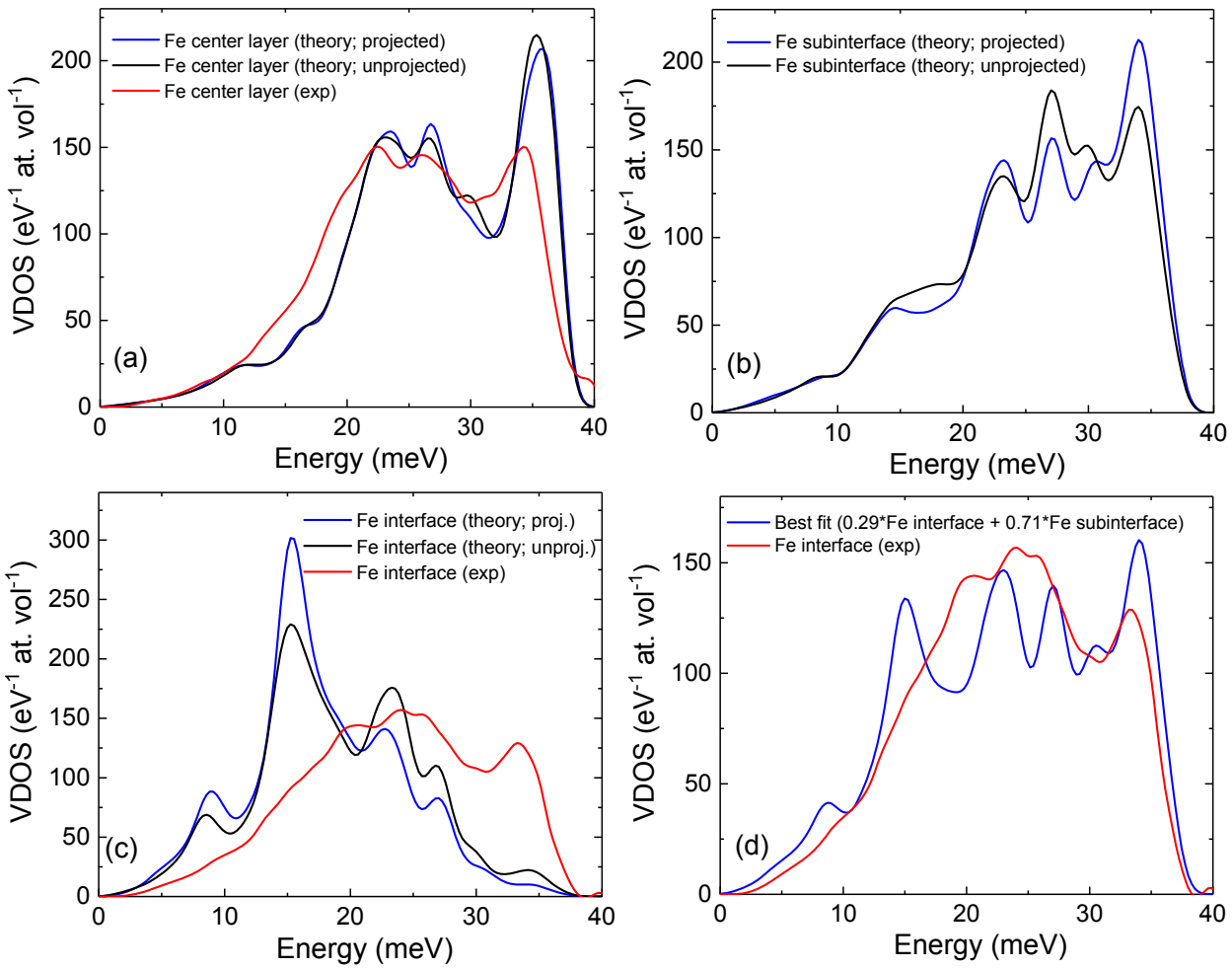

FIG. 9: (Color online) A comparison among unprojected (from Fig. 4(c)) and direction-projected theoretical Fe-VDOS and experimental Fe-VDOS (from Fig. 3(a)) for Fe/Ag(001) multilayers. The areas below the theoretical VDOS curves are normalized according to the experimental VDOS**. (a)** The theoretical unprojected (black line) and projected (blue line) Fe-VDOS of Fe/Ag(001) at the center (Fe layer 4 in Fig. 4(c)) together with the experimental (red line) VDOS for the Fe center layer in Fe/Ag); **(b)** the unprojected (black line) and projected (blue line) theoretical Fe-VDOS of the Fe/Ag(001) subinterface (Fe layer 2 in Fig. 4(c)). **(c)** The theoretical unprojected (black line) and projected (blue line) Fe-VDOS of Fe/Ag(001) at the interface (Fe layer 1 in Fig. 4(c)) together with the experimental (red line) VDOS 4 for the Fe/Ag interface sample) **(d)** Best-fit of the experimental interface VDOS (red line) by the sum of the theoretical projected Fe interface and subinterface layer VDOS. The best fit (blue line) can be obtained by mixing 29 % of the calculated interface VDOS and 71 % of the calculated subinterface VDOS.